METHODS

Renilla luciferase influenza virus

The coding region for the viral hemagglutinin (HA) protein was replaced with that of *Renilla* luciferase and the packaging signals for the HA segment were added to either end, as described in Marsh *et al* [29]. The recombinant WSN-Ren virus was generated by reverse genetics in the presence of complementing HA and amplified in HA-expressing MDCK cells [29].

siRNA libraries

The following commercially available siRNA libaries were used in this study: the whole-genome library from Qiagen (Druggable Set version 2 (approx. 7000 genes targeted by ~28000 siRNA constructs), NM Set version 1 (approx. 10000 genes targeted by ~42000 constructs) and XM Set version 1 (approx. 5300 genes targeted by ~21000 constructs), the kinome library from Invitrogen (1287 siRNAs targeting 636 genes) and the kinome library from IDT (2176 siRNAs targeting 542 genes). In addition, druggable genome library version 1 from Qiagen, which is no longer commercially available, was used (approx. 5000 genes targeted by ~10000 siRNAs). All sequences for siRNAs targeting influenza virus host proteins can be found in Supplemental Table S1.

RNAi screen

A 384-well plate-based assay was optimized to identify siRNAs that influence infection of human A549 cells by WSN-Ren virus. A toxicity assay was optimized to identify

siRNAs that influence cell viability. The optimal ratio of the effect of the positive control siRNA (siRenilla (Ambion, AM4630) for the viral screen and siRPS27a (5'-AAGCUGGAAGAUGGACGUACU-3') to that of two negative control siRNA (scramble177 5'-GGTAATTGCGCGTGCAACT-3' and scramble5701 5'-GCCGCTTAGTAGTCTCGTA-3') were used to optimize the assay conditions.

Genome-wide libraries comprising 98,737 synthetic siRNAs targeting 19,628 unique human genes in total were arrayed in 384-well plates (7ng/siRNA) such that each well contained either two (47,560 wells) or one (3617 wells) unique and identifiable siRNA per gene). On average, there were 3 wells/gene or 6 siRNAs/gene. Each plate also contained the positive and the negative control siRNAs as indicated above. The library matrix was introduced into A549 cells through a high throughput transfection process [30,31]. 1pmol siRNA was incubated at RT for 20 min with 50nl RNAimax in 20ul opti-mem/well and then transfected into 1500 A549 cells in 10 ul DMEM supplemented with 10% FBS and antibiotics. For the viral screen, after 48h, the cells were infected at a multiplicity of infection (MOI) of 0.5 in 10 ul serum-free DMEM containing 0.875 ug/ml final concentration Trypsin (Sigma). After 5 hours, EnduRen Life Cell substrate (Promega) was added at a final concentration of 10 uM in 10 ul serum-free DMEM. Relative luminescence for each well was analyzed on a 384-well plate reader (Viewlux) at 12h, 24h and 36h after infection. The screen was run twice (in independent experiments) to generate duplicate results and statistically analyzed as described

below. All steps were performed using a fully integrated high-throughput cellular genomics robotic system (GNF Systems; www.gnfsystems.com).

To enable consistent comparison between assays, we have developed a scaling methodology that sets the positive control (siRNA against luciferase) at an arbitrary value of 0.1, and our negative control siRNAs at 1. Luciferase activities of siRNAs targeting host factors are assigned a score based on the distribution of these values.

Bioinformatic analysis of screening data

Evidence Analyses

We assume that screening hits with multiple lines of independent indications for influenza virus-related functions are less likely to be a false positive. Such a multi-evidence strategy has been validated in a previous study in its successful identification of novel HIV host factors [4]. The evidence collected for this study is described below, and a summary of data processing is found in the proceeding flowchart.
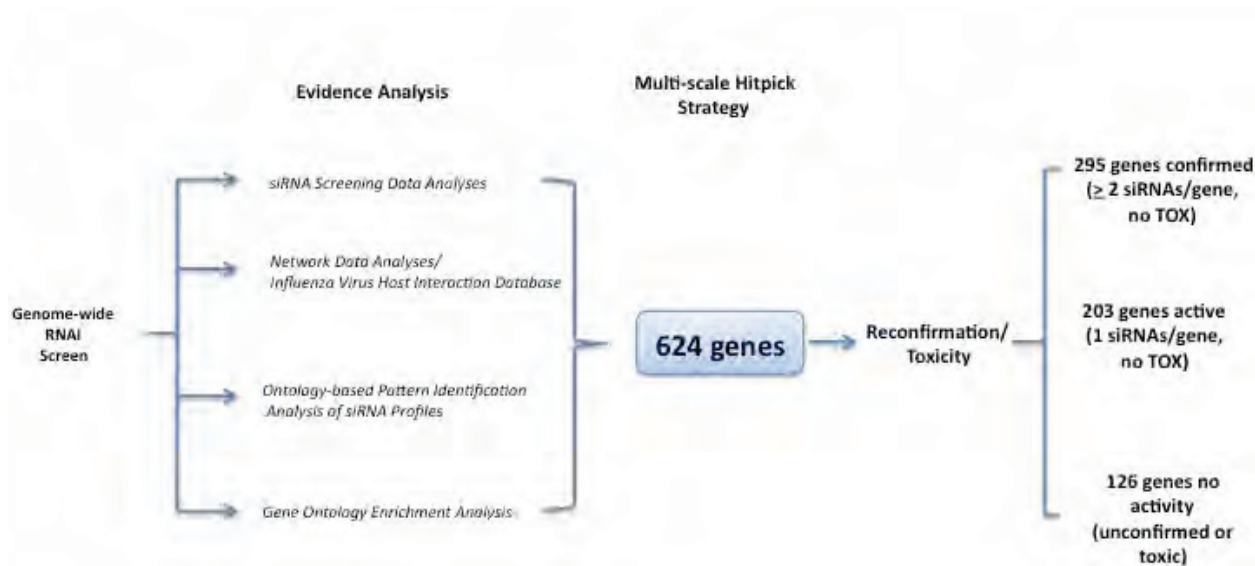
siRNA Screening Data Analyses

Screening data were normalized as previously described [32]. The activity score for each gene in an assay was taken from the most potent siRNA per gene. Each screen was then analyzed using a Redundant siRNA Analysis (RSA) algorithm [32] and a p-value was assigned to each gene in a screen. The RSA p-value represents the likelihood of the corresponding siRNA signal distribution to be generated by chance, i.e., the smaller the p-value, the higher the expected confirmation rate [32]. The minimum score of a gene among the 12h-, 24h-, and 36h- A549 assays was chosen as the A549 activity score for the gene. With a hit criterion of an activity score <0.4, 1936 genes were defined as primary hits for the A549 influenza virus screen (see next section "Network Data Analyses").

Network Data Analyses

The analysis was based on protein-protein binding data derived from Yeast-two-Hybrid databases including published datasets [23, 24], Hynet (http://www.ariadnegenomics.com/products/databases/prolexys-hynet/) and curated molecular interaction databases including Reactome (http://reactome.org), BIND (http://www.bind.ca), MINT (http://mint.bio.uniroma2.it/mint/) and HPRD (http://www.hprd.org). Among all the 1936 primary A549 hits, 1472 proteins form 81122 direct or indirect interactions (interact through a third protein) among themselves (p < 0.001) and 968 proteins form 2160 direct interactions among themselves (p < 0.001). In order to identify densely-connected local network neighborhoods, we carried out Molecular Complex Detection (MCODE) analysis and identified 18 subnetworks[25]. The membership of a primary hit in these networks was considered a favorable piece of evidence.

Influenza Virus Host Interaction Database

We identified 101 host proteins that form 111 interactions with 11 influenza virus proteins or protein complexes from previously reported publications. Using the protein-protein network described above, we expand the list to include those proteins that interact with an influenza virus protein through another human protein based on the following references: [33-36, 37-72].

Ontology-based Pattern Identification Analysis of siRNA Profiles

For all genes screened in our study, a data matrix was constructed based on inhibition across several biological assays: three A549 assays were screened at 12h, 24h and 36h, and four assays from a previous HIV study (HIV, MMLV, adeno-associated virus (AAV), and toxicity assays) using the same screening library[4]. Ontology-based Pattern Identification (OPI) is an algorithm that has been previously successfully applied to either predict gene functions based on their expression patterns [73, 74], or prioritize genes based on their phenotypic patterns [75]. Here we applied the algorithm to identify gene clusters that not only share similar inhibition patterns, but also show statistical enrichment in certain functional categories. OPI clustering analysis on the 1449 genes resulted in 163 statistically significant clusters with permutation-based p-values ≤ 0.05 and cluster size ≤ 500. Therefore, genes that fall into any statistically significant OPI cluster were assigned a supporting score of 0.5. Additionally, we conducted a false discovery rate (FDR) analysis for each cluster, and those that fell below 0.5 were assigned a supporting score of 1.0, to reflect this additional stringency.

Gene Ontology Enrichment Analysis

P-values of functional enrichment analyses using accumulated hypergeometric distribution[73] were calculated on the primary hit lists. All gene members of GO groups with p-values less than 10^{-10} are considered to provide support for each other. The same analysis routine was also applied to hit lists from other viral screens to identify shared biological processes (Figure S8).

Multi-scale Strategy

We combined all the evidence described above and normalized each evidence score, so that 0 means no support and 1 means the best level of support. In such a systems-based approach, data from functional genomics screens, protein-protein interaction networks, and human-influenza virus interaction datasets were combined, so that true (biologically relevant) positive genes that have multiple lines of evidence to support their activities have a better chance to be identified. The evidence matrix was then hierarchically clustered, so that primary hits were segregated into various evidence patterns and candidates were selected based on the biological relevance of their corresponding evidence profiles for reconfirmation. The evidence matrix for confirmed host factors is shown in Table S1.

Reconfirmation screens

siRNAs for reconfirmation of 624 genes were individually rearrayed such that each well of a 384-well plate contained a single siRNA (7 ng). 43 scrambled negative controls [32] were added to each plate in quadruplicate in addition to 3 commercially available controls (negative control GL2-Luciferase (Dharmacon), All-Star Negative Control (Qiagen) and Negative Control siRNA (Qiagen)) and the respective positive controls. The influenza virus infection assay was rerun as previously described. Additionally a parallel assay was run to assess potential cellular toxicity induced by the siRNA through

addition of CellTiterGlo (Promega) detection reagent 72 hours after transfection. Each siRNA was screened a minimum of three times for each readout, in at least two independent assay runs.

CellTiterGlo is a robust and sensitive reagent for measuring cellular viability in high-throughput conditions. However, since it relies upon the measurement of intracellular ATP levels as a surrogate for cell counts, certain RNAi activities may be directly regulating ATP levels, for example through modulation of cellular metabolic processes or mitochondrial function, and thus be inappropriately classified as toxic.

The results from the influenza virus infection assay were analyzed such that an siRNA was considered to be confirmed only if the median signal of all readings was below 0.65 (~35% reduction). A gene was considered a true positive if there were at least two independent siRNAs confirmed based on this criterion, and that it met the toxicity criterion as described below.

Toxicity filtering strategy

For the toxic control siRNA - siRPS27a, titration data series were measured for both infectivity assays and toxicity assays in 5 replicates. To estimate experimental noise level, each data series was curve-fitted using the standard sigmoidal model as defined:

$$score = bottom + \frac{top - bottom}{1 + (\frac{IC_{50}}{concentration})^{slope}} \, , (1)$$

where bottom is reflected by a score of approximately 0, while top is reflected by the approximate score of 1. IC_{50} is the siRNA concentration corresponding to the score

representing 50% inhibition (around score 0.5), slope is a negative value representing Hill slope, score is the measured normalized activity value. Both data points and curve parameters were then linearly transformed so that all curves sit at a bottom value of 0 and a top value of 1. From the residue of the curve fitting, the intrinsic data noise in the experiment can be estimated as ε_T and ε_I for the toxicity assay and the infectivity assay, respectively.

The five infectivity curves and five toxicity curves form 25 unbiased toxicity-infectivity (*T-I*) relationship pairs, i.e.,

$$\text{Toxicity}(c) = \frac{1}{1+(\frac{TOX_{50}}{c})^{TOXslope}} + \varepsilon_T \quad (2)$$

$$\text{Infectivity}(c) = \frac{1}{1+(\frac{INF_{50}}{c})^{INFslope}} + \varepsilon_I \quad (3)$$

With increasing concentration of siRNA (zero to infinity), *c*, a series of infectivity and toxicity scores were determined. The boundary represents the average infectivity score for any given toxicity score, if the siRNA is toxic.

The next step was to establish the infectivity confidence threshold for any given toxicity score, so that the boundary is below 95% of the possible infectivity scores produced by a random toxic siRNA. If an siRNA of interest produces an infectivity score below the established threshold (lower score means higher activity), the false positive p-value is below 0.05. This can be simulated by using the Gaussian noise term ε_T and ε_I in equation (2) and (3).

More specifically, for any given observed toxicity score T between 0 and 1, at the incremental size of 0.01, we generated 1000 true toxicity scores based on the Bayesian probability of their occurrence, simulated based on equation (2). Each simulated true toxicity score then led to a true concentration c, and resulted in 1000 infectivity scores I according to equation (3). The 95 percentiles of the 1,000,000 simulated infectivity scores for each given observed toxicity score are used to construct the decision boundary.

Figure S1 shows the decision boundary as a green curve. When an siRNA falls into the region above the boundary, its effect on infectivity is unlikely to be caused by toxicity ($p < 0.05$). When a toxicity score is <0.34, the infectivity score of an siRNA is highly likely to be affected by its toxicity, indicated by the flat horizontal line segment in the upper right corner of the plot. As toxicity scores get larger (weak toxicity) and the corresponding infectivity score is sufficiently low (above the green curve), the effect of the siRNA on infectivity is most likely to be true. We also verified that the T-I data points from our positive control siRenilla (green circles) had most data points above the decision boundary showing the siRNA is a true hit, while toxic controls (pink circles for siRPS27a) fall below the decision boundary. The non-toxic negative control scrambled siRNA falls mostly below the decision boundary. Although some controls slightly cross the boundary at the high infectivity score end (weak infectivity and toxicity), they all fall into a region where infectivity score > 0.6, which means that these siRNAs will not be hit picked and therefore do not introduce decision errors.

Bioinformatic analysis of confirmed factors

Network Analysis

A protein-protein interaction network was first constructed with 262 confirmed genes and 377 putative host factors based on binary protein interaction data derived from publicly available databases including BIND, HPRD, MINT, Reactome, Rual et al.[23], and Stelzl et al.[24], curated protein complex data (CORUM), the Hynet yeast two-hybrid database, and virus-host interaction data derived from the literature (see *Influenza Virus Host Interaction Database*). Putative host factors refer to those that were not experimentally confirmed, but nevertheless interacted with at least two confirmed host genes and had an activity score < 0.6. MCODE analysis was performed and 17 densely connected components consisting of 224 genes were identified. Another 152 confirmed genes not in the MCODE network were added back to the network, as they formed direct interactions with the MCODE members. The final network (Figure 1c) consists of 181 confirmed host genes, 10 viral nodes, and 184 putative host genes. Viral nodes were abbreviated as follows: HA (Hemagglutinin), NS1 (NS1 protein), M1 (M1 Matrix protein), NEP (NEP/NS2 protein), NP (NP protein), PB1 and PB2 (the polymerase subunits PB1 and PB2), PB1-F2 (PB1-F2 protein), vRNP (influenza viral ribonucleoprotein complex), virion (proteins incorporated into virions).

Comparative Analysis of Host Factor Complex Usage.

We adopted four approaches in identifying network clusters to avoid bias introduced by any particular algorithm. (1) The 17 MCODE clusters identified from the confirmed gene network, as described previously (Figures 2b, 2c, 2g, 2h, 3b, S5) were considered. (2)

We next derived a binary distance matrix from the initial whole human network (13,770 proteins, 131,559 interactions), where a matrix element of one represents an interaction between two proteins, zero for no interaction. The matrix was then used to drive a hierarchically cluster analysis; the 13,770 proteins were partitioned into densely connected clusters. A total of 85 clusters having at least five protein members were obtained. (3) Hits from all viral screens were merged into an interaction network of 1,052 proteins and 4,398 interactions. A total of 20 MCODE clusters were identified therein. (4) For the same protein network, we constructed a binary distance matrix and hierarchically clustered and partitioned the hits. A total of 30 clusters having at least three protein members were obtained.

Among all the clusters obtained above, 77 clusters were found to be enriched in certain GO categories ($p < 10^{-4}$) and considered to be biologically interpretable. These clusters were further analyzed for their enrichment (using the accumulative hypergeometric p-value which compares the number of genes overlapping between a module and a particular screen to that which would be expected by chance) across viral screen hit lists. A subset of 38 clusters is shown in Figure 1d.

Hub and CORUM (Known Biochemical Complex) Analysis

We evaluated whether proteins found to be essential for infection by the influenza virus were more likely to be 'hub' proteins in a protein interaction network as well as more likely to be a component of a known protein complex. We culled multiple public databases of human protein interactions into a list of 57,263 unique human protein interactions (previously described). We found that proteins whose corresponding genes

were identified in this study had a significantly higher mean and median number of protein interactions than background. In the case of the mean, the influenza set had an average of 18.75 protein interaction partners, nearly double that expected by chance (9.925), which was highly significant as assessed by a Student's t-test. As for the median, the influenza virus set had a median of 8 protein interaction partners, double that expected by chance (4), which was highly significant as assessed by a rank sum test. We also found similar trends for other published viral siRNA screens (data not shown). We also evaluated whether influenza virus preferentially targets members of protein complexes rather than proteins which do not act in large macromolecular structures. Using the CORUM database of human protein complexes covering 2,072 proteins, or roughly 7% of the human genome, we found a significant enrichment of host cell factors which were members of a known protein complex (16.6%, p=2.7x10-7 via hypergeometric test). Together, these results suggest that one mechanism for viral infection is to hijack central nodes, or major players in cellular networks in order to increase the efficacy of infection. Data are shown in Supplemental Figure S6.

Selection for hit criteria

The criteria for selection at each stage of the screen progress are as follows (Fig. 2a): (i) A multi-scale strategy was applied to the genome-wide analysis (see Methods and Flow-chart). After reconfirmation analysis, we selected genes with at least 2 siRNAs that resulted in a 35% (~ 2 SD) or greater decrease in influenza virus reporter activity, without concomitant induction of cytotoxicity. (*ii*) WT influenza virus multi-cycle growth

analyzed by hemagglutination assay: >4 fold reduction of wild-type influenza virus multi-cycle growth using at least 2 siRNAs targeting the same gene and (*iii*) Viral gene expression analyzed by quantitative RT-PCR of NP and M1 influenza protein: transfection of 1 or more siRNAs per gene resulting in a 35% or greater decrease in influenza virus NP and M1 RNA transcription. Functional assays (iv) were employed to characterize several of the host factors (validated in the HA-assay) in entry and post-entry steps of virus replication include: pseudotyped particle entry assay (pH-dependent/-independent), Bla-M1 influenza VLP entry assay, NP localization at 90 and 180min post-infection and influenza mini-genome replication assay (see text and supplemental materials). Of the 45 factors tested in functional assays, 12 did not meet the criteria for classification.

Cells and viruses

A549 cells, 293T cells, Vero cells and MDCK cells were maintained in Dulbecco's minimal essential medium containing antibiotics and 10% fetal bovine serum at 37°C and 5% CO_2. Generation of and maintenance of MDCK cells expressing the HA protein of influenza A/WSN/33 virus was described previously [29].

Influenza A virus A/WSN/33 and swine origin influenza A/Netherlands/602/2009 virus (SOIV) were grown in MDCK cells. Virus stocks were titered by plaque assay on MDCK cells. Vesicular stomatitis virus (VSV) was grown and titered in Vero cells. The WSN-Ren virus was grown and titered in MDCK-HA cells.

siRNA transfections of A549 cells

A549 cells (passage 2-15) were transfected with siRNAs at a concentration of 30 nM in a reverse transfection procedure using RNAiMAX (Invitrogen, Carlsbad, CA). Knockdown was allowed to proceed for 48h before cells were infected or tested in functional assays.

Screen for inhibition of WT influenza virus growth

A549 cells were transfected with siRNAs as described above. At 48h post transfection cells were infected with influenza A/WSN/33 virus at a multiplicity of infection (MOI) of 0.01. At 36h post infection supernatants were harvested and titered by hemagglutination assay (HA assay). In brief, two-fold serial dilutions of the supernatant were incubated with chicken red blood cells at a final concentration of 0.25% for 60 min on ice. For each gene at least two different siRNAs were tested individually and the gene was called a required host factor if there was a difference of at least four-fold in hemagglutination titer for two or more siRNAs. Values for WSN WT in Figures 2b and 3a represent the mean of 2 replicates.

Quantitative RT-PCR

A549 cells were reverse transfected with siRNAs using Lipofectamine RNAiMAX reagent (Invitrogen) in 96 well plates. Briefly, 2 pmol siRNAs were diluted in 20 ul of Opti-MEM (Invitrogen) and mixed with 200 nl of Lipofectamine RNAiMAX with 20 ul Opti-MEM for 20 min. A549 cells (2×10^5 cells/ml) in 60 ul DMEM containing 10% FBS were added to each well. 48 h after transfection, influenza A/PR/8/34 virus (MOI = 0.5)

and TPCK trypsin (50 ng; 0.9 ug/ml final) in 10 ul of DMEM were added to cells. 8 h after infection, RNA samples were isolated using RNeasy 96 Total RNA Isolation kit (Qiagen).

For cDNA synthesis, QuantiTect Reverse Transcription Kit (Qiagen) was used in accordance to the manufacturer's protocol.

Real-time PCR was performed using SYBR Green PCR Master Mix (Applied Biosystems) with the primer sequences described below. IFNb: sense primer sequence 5′-TGACATCCCTGAGGAGATTAAGC-3′ and antisense primer sequence 5′-CTGGAGCATCTCATAGATGGTCAAT-3′. PR8 NP: sense primer sequence 5′-TGGCATTCCAATTTGAATGAT-3′ and antisense primer sequence 5′-ATCCATTCCGGTGCGAACAAG-3′. PR8 M1: sense primer sequence 5′-CCGTCGCTTTAAATACGGACT-3′ and antisense primer sequence 5′-AGCACTCTGCTGTTCCTTTCG-3′. GAPDH was selected as the endogenous control gene and was amplified using sense primer sequence 5′-GAAGATGGTGATGGGATTTC-3′ and antisense primer sequence 5′-GAAGGTGAAGGTCGGAGTC-3′.

Primers for analyzing knock-down efficiency of siRNA treatment were as follows:

gene name	sense or antisense primer	primer sequence 5'-3'
ARCN	sense	GGGGTGCTAAAGTGGAGACTAC
ARCN	antisense	CACAGCCATTTCCACTCTCC
ATP6VOC	sense	CCCGAGTATGCTTCGTTTTTCG
ATP6VOC	antisense	CATGACCACTGGGATGATGGA
CD81	sense	TTCCACGAGACGCTTGACTG

CD81	antisense	CTTCCCGGAGAAGAGGTCATC
CSE1L	sense	CAGAACACGCTGACAAGTATCT
CSE1L	antisense	AGCCCTGCGTCTAGTATCAATA
FGFR4v1	sense	AGGCCTCTGAGGAAGTGGA
FGFR4v1	antisense	CTGCCCAAGGGCTACTGTC
GABBR1	sense	CCCGACTTCCATCTGGTG
GABBR1	antisense	GTGGCGTTCGATTCACCT
GSK3B	sense	ATTTCCAGGGGATAGTGGTGT
GSK3B	antisense	GGTCGGAAGACCTTAGTCCAAG
MAP2K3	sense	GGAGGCTGATGACTTGGTGAC
MAP2K3	antisense	CTGCTCCTGTGAGTTCACGG
PRSS35	sense	CCCTGGGTGGACCCTCATT
PRSS35	antisense	CATTCGATGCCACACACTGTAT
MID1IP1	sense	ACAGCCACTACGTGCTTCTC
MID1IP1	antisense	CTTTGCGCGTGAGTTTCGAG
SUMO2	sense	GAAAGCCTATTGTGAACGACAGT
SUMO2	antisense	TCTGCTGTTGGAACACATCAA
CAMK2B	sense	CCTACGCGAAAATCTGTGACC
CAMK2B	antisense	TGGAAGTCCATCCCTTCAACC

cDNA samples were amplified under standard thermal cycler protocol (50 °C for 2 min, 95 °C for 10 min, and 40 cycles of 95 °C for 15 s and 60 °C for 1 min). Relative expression level was calculated using the endogenous control GAPDH. Fold changes were calculated against the median of negative control siRNAs, scramble 177 (5'-GGTAATTGCGCGTGCAACT-3'), 1212 (5'-ATCCGCGCGATAGTACGTA-3'), 6105 (5'-GTAAGCTCGTGCGACGTAT-3'), siGL2 (Dharmacon), siGL3 (Dharmacon) and siGFP-22 (Qiagen). Each value for relative expression levels in supplemental tables S9 and S10 (and Fig. 2b and 3a) represent the average of at least 2 independent results. The relative expression levels in Supplemental Table S13 are comprised of the average of 4 replicates.

Entry assays

Pseudoparticles bearing different viral envelopes were used to elucidate genes involved in influenza virus entry. Specifically, siRNA-transfected A549 cells were incubated with an appropriate dilution of different pseudoparticles for one hour. The inoculum was removed, medium was added back and cells were incubated for 36h. Entry efficiency was measured as the amount of luciferase secreted into the supernatant (Renilla Luciferase Assay System, Promega, Madison, WI). A gene was considered a hit in the pseudoparticle assay if one siRNA reduced luciferase signal by at least 65% compared to a scrambled control siRNA and a second siRNA resulted in a reduction of at least 50%. Pseudoparticles were generated by transfecting 293T cells with plasmids encoding (1) a minimal HIV provirus encoding the Gaussia luciferase reporter gene (2) HIV gag-pol and (3) a viral envelope protein (WSN-HA/NA, VSV-G or MMLV env) using FuGENE6 (Roche Applied Science, Indianapolis). Each datapoint in figure 2b and 3a represents the mean of at least 3 replicates.

The beta-lactamase-M1 (Bla-M1) virus-like particle (VLP) assay was performed as follows: Bla-M1 VLPs contain WSN HA, NA, and a Bla-M1 fusion protein, which is packaged as a structural component into the VLP and released upon fusion with the target cell. siRNA-transfected A549 cells were incubated with the Bla-M1 VLPs and centrifuged at 1.5 k rpm, for 90 min at 4°C. The cells were then transferred to 37°C and incubated an additional 3-4 h. To detect beta-lactamase activity by flow cytometry, cells were detached and loaded with CCF2-AM substrate (Invitrogen). Flow cytometry was performed at the Mount Sinai Flow Cytometry Shared Resource Facility on an LSRII

flow cytometer (Becton Dickinson, Miami, FL). Samples were gated on live cells and analyzed for their cleavage of CCF2 using FlowJo 8.5.2 software.

Influenza mini-genome assay

For the minigenome assay, 293T cells were transfected with siRNAs as described for A549 cells. At 48h post transfection, cells were transfected with plasmids encoding the three polymerase subunits and the nucleoprotein of influenza virus A/WSN/33, the reporter construct pPOLI-Luc-RT, encoding firefly luciferase in the negative-sense orientation flanked by the noncoding regions of segment 8 of strain A/WSN/33 [76] as well as the control reporter plasmid pRL-SV40-R*luc* (Promega, Madison, WI). The amounts of polymerase encoding plasmids were titrated to achieve 50% of the system's maximum activity. At 36h post transfection reporter activity was determined using the Dual-Glo Luciferase Assays system (Promega, Madison, WI). Each datapoint in Figure 3c represents the mean of at least 6 replicates.

Immunofluorescence

At 48h post transfection siRNA-treated A549 cells were pre-chilled for 15 min on ice, washed with cold PBS and then infected with influenza virus A/WSN/33 at an MOI of 10 for 45 min on ice to synchronize the infection. Unbound virus was removed by three washes with cold PBS. Pre-warmed medium was added and cells were incubated at 37°C. At different time points post infection cells were fixed with 3% paraformaldehyde for 15 min at room temperature (RT) and subsequently permeabilized with 0.5% Triton-X-100 for 5 min at RT. Immunofluorescence staining was performed using the mouse monoclonal antibody HT103 against influenza A virus nucleoprotein [77] as a primary

antibody and a donkey anti-mouse Alexa 488 secondary antibody (Invitrogen, Carlsbad, CA). In addition, nuclei were stained with DAPI (Invitrogen, Carlsbad, CA). Confocal laser scanning microscopy was performed at the MSSM-Microscopy Shared Resource Facility, supported with funding from NIH-NCI shared resources grant (5R24 CA095823-04), NSF Major Research Instrumentation grant (DBI-9724504) and NIH shared instrumentation grant (1 S10 RR0 9145-01).

Immunofluoresence of EEA1 and influenza virus particles

A549 cells on coverslips were reverse transfected with 30nM ATP6V0C siRNA or 5757 negative control siRNA (5'- GGTGCTCAGTCGCAATAGT'3'). 48h post transfection, WSN virus was added to the cells at an MOI of 1 for 20 mins. The cells were then fixed with 4% PFA in PBS. WSN-HA was stained with a mouse monoclonal antibody; 2G9D1 (Palese lab, MSSM) and Cy3 conjugated secondary antibody (Jackson ImmunoResearch). Early endosomes were stained with a rabbit polyclonal EEA1 antibody (Abcam) and Cy5 conjugated secondary antibody (Jackson ImmunoResearch). DNA was stained with DAPI. The coverslips were imaged at 100X magnification and z stacks were collected using an Olympus FV1000 confocal microscope. The total number of HA positive virions in a single cell were manually counted.

High Content Imaging

The high-content imaging-based analysis was performed using the Opera (Perkin-Elmer, Waltham, MA), a fully automated confocal microscope system. 384-well plates containing cells transfected with various siRNAs were exposed to the virus (MOI = 5)

and fixed at three different time points (T=0', T=90' and T=180'). After immunofluorescence labeling (as previously described), cells were imaged using a 20X 0.7NA Water immersion lens (Olympus, Japan). A total of 10-11 images for both the nuclear stain (Hoechst) and the Alexa488 labeled WSN-NP were taken in each well.

Cellular features were then extracted from the images using a custom Acapella script (Perkin-Elmer), and the median value for each of these features was calculated to provide a well-level feature set. The ratio of nuclear versus cytoplasmic WSN-NP intensity (Nuc/Cyto ratio) was determined. The mean value and the standard deviation was calculated for each siRNA and each time point. The non-targeting siRNAs for which Nuc/Cyto ratio was four standard deviations away from the mean were discarded as outliers. A Welch TTest was then performed between each siRNA and non-targeting siRNAs. The siRNAs with pValue<0.01 and at least a 15% difference in signal from controls were selected as relevant and imaged again with the Opera this time using a 40x 0.9NA water immersion lens (Olympus). Representative images were selected from the 10 images collected in the different controls (Supplementary Figure S11). Data shown in Figure 3a were generated by background subtraction of all values using the scrambled negative control measurements at 0' as a baseline (negative values were set to 0.001), and then scaled such that the negative control 180' value equaled 1.

Small molecule inhibitors

HSP90 Inhibitor, CCT018159 (Calbiochem), Podophyllotoxin (MP Biomedicals), FGF/VEGF Receptor Tyrosine Kinase Inhibitor (Calbiochem, 341607), Sirolimus (LC Laboratories), Hymenialdisine (Biomol International LP), Betulinic Acid (VWR

International (Enzo Life Sciences Intl)), were dissolved in their respective diluent DMSO or ethanol (for Podophyllotoxin) and titrated in DMSO starting from 100 uM. Inhibition of WSN-Ren virus growth in MDCK-HA cells was determined by Renilla luciferase activity at 36h post infection (or 24h post infection for Sirolimus). Cellular toxicity was determined by CellTiterGlo assay (Promega Corp., Madison, WI).

Diphyllin was identified in a high-throughput screen of small molecular weight compounds as having influenza virus inhibitory activity. The screen assay was described previously [78] and diphyllin was identified from a library supplied by ChemDiv (San Diego, CA). The screen was performed at the National Screening Laboratory for the Regional Centers of Excellence in Biodefense (NSRB), Harvard Medical School, Boston and was supported by NIH grant U54 AI057159.

Diphyllin and KN-93 were purchased from Sigma and Calbiochem, respectively and dissolved in DMSO. Cellular toxicity was determined by the CellTiterGlo assay (Promega Corp., Madison, WI) and inhibition of virus growth was determined by standard plaque assay.

Interferon Bioassay

48 hours after transfection of siRNAs, A549 cells were either mock treated or infected with influenza A/PR/8/34 virus (MOI=3). Control samples were also infected with a recombinant PR/8/34 virus expressing a truncated NS1 protein (residues 1-113), as a positive control for IFN induction. After 1 hour of adsorption, DMEM containing 10% fetal calf serum was added, and the cells incubated for 18 hours at 37°C in 5% CO_2. Levels of interferon secreted by the cells were determined as previously described [79]

with some variations. At 18 hours post infection, supernatants were harvested and virus present in the supernatant was UV inactivated by placing the 96-well plate in a UV chamber delivering 200 J/cm^2. 2-fold dilutions of the inactivated supernatants were added to Vero cells previously seeded in 96-well plates. Following a 24h incubation the Vero cells were infected with a GFP-expressing Newcastle disease virus (NDV-GFP) [80]. Cells expressing GFP were visualized 24h post infection by fluorescence microscopy. Each image was analyzed with the software ImageJ (NIH) and the Mean Fluorescence Value per unit area of each image was calculated.

Inhibition of virus growth

siRNA-transfected A549 cells were infected with either influenza A/WSN/33 virus or VSV at a multiplicity of infection (MOI) of 0.01 or swine origin influenza A/Netherlands/602/2009 virus (SOIV) at an MOI of 1 at 48h post siRNA transfection. At 36h post infection supernatants were harvested and virus titers were determined by plaque assay on MDCK cells (for A/WSN/33 and A/Netherlands/602/2009) or on Vero cells for VSV. Each sample in Figure 3e is represented by at least 3 replicates.

References

1. Ashburner, M. *et al.* Gene ontology: tool for the unification of biology. The Gene Ontology Consortium. *Nat Genet* **25**, 25-29 (2000).
2. Apweiler, R. *et al.* The InterPro database, an integrated documentation resource for protein families, domains and functional sites. *Nucleic acids research* **29**, 37-40 (2001).
3. Huss, J.W., 3rd *et al.* A gene wiki for community annotation of gene function. *PLoS Biol* **6**, e175 (2008).
4. Konig, R. *et al.* Global analysis of host-pathogen interactions that regulate early-stage HIV-1 replication. *Cell* **135**, 49-60 (2008).
5. Krishnan, M.N. *et al.* RNA interference screen for human genes associated with West Nile virus infection. *Nature* **455**, 242-245 (2008).

6. Tai, A.W. *et al.* A functional genomic screen identifies cellular cofactors of hepatitis C virus replication. *Cell Host Microbe* **5**, 298-307 (2009).

7. Sessions, O.M. *et al.* Discovery of insect and human dengue virus host factors. *Nature* **458**, 1047-1050 (2009).

8. Hao, L. *et al.* Drosophila RNAi screen identifies host genes important for influenza virus replication. *Nature* **454**, 890-893 (2008).

9. Sui, B. *et al.* The use of Random Homozygous Gene Perturbation to identify novel host-oriented targets for influenza. *Virology* **387**, 473-481 (2009).

10. Huang da, W., Sherman, B.T. & Lempicki, R.A. Systematic and integrative analysis of large gene lists using DAVID bioinformatics resources. *Nat Protoc* **4**, 44-57 (2009).

11. Terada, N. *et al.* Rapamycin inhibits the phosphorylation of p70 S6 kinase in IL-2 and mitogen-activated human T cells. *Biochem Biophys Res Commun* **186**, 1315-1321 (1992).

12. Price, D.J., Grove, J.R., Calvo, V., Avruch, J. & Bierer, B.E. Rapamycin-induced inhibition of the 70-kilodalton S6 protein kinase. *Science* **257**, 973-977 (1992).

13. Chung, J., Kuo, C.J., Crabtree, G.R. & Blenis, J. Rapamycin-FKBP specifically blocks growth-dependent activation of and signaling by the 70 kd S6 protein kinases. *Cell* **69**, 1227-1236 (1992).

14. Hardcastle, A. *et al.* Solid-phase immunoassays in mechanism-based drug discovery: their application in the development of inhibitors of the molecular chaperone heat-shock protein 90. *Assay Drug Dev Technol* **3**, 273-285 (2005).

15. Sharp, S.Y. *et al.* In vitro biological characterization of a novel, synthetic diaryl pyrazole resorcinol class of heat shock protein 90 inhibitors. *Cancer Res* **67**, 2206-2216 (2007).

16. Smith, N.F. *et al.* Preclinical pharmacokinetics and metabolism of a novel diaryl pyrazole resorcinol series of heat shock protein 90 inhibitors. *Mol Cancer Ther* **5**, 1628-1637 (2006).

17. Desbene, S. & Giorgi-Renault, S. Drugs that inhibit tubulin polymerization: the particular case of podophyllotoxin and analogues. *Curr Med Chem Anticancer Agents* **2**, 71-90 (2002).

18. Renhowe, P.A. *et al.* Design, structure-activity relationships and in vivo characterization of 4-amino-3-benzimidazol-2-ylhydroquinolin-2-ones: a novel class of receptor tyrosine kinase inhibitors. *J Med Chem* **52**, 278-292 (2009).

19. Supriyono, A. *et al.* Bioactive alkaloids from the tropical marine sponge Axinella carteri. *Z Naturforsch C* **50**, 669-674 (1995).

20. Meijer, L. *et al.* Inhibition of cyclin-dependent kinases, GSK-3beta and CK1 by hymenialdisine, a marine sponge constituent. *Chem Biol* **7**, 51-63 (2000).

21. Melzig, M.F. & Bormann, H. Betulinic acid inhibits aminopeptidase N activity. *Planta Med* **64**, 655-657 (1998).

22. Chase, G. *et al.* Hsp90 inhibitors reduce influenza virus replication in cell culture. *Virology* **377**, 431-439 (2008).

23. Rual, J.F. *et al.* Towards a proteome-scale map of the human protein-protein interaction network. *Nature* **437**, 1173-1178 (2005).

24. Stelzl, U. *et al.* A human protein-protein interaction network: a resource for annotating the proteome. *Cell* **122**, 957-968 (2005).

25. Bader, G.D. & Hogue, C.W. An automated method for finding molecular complexes in large protein interaction networks. *BMC Bioinformatics* **4**, 2 (2003).

26. Zhou, H. *et al.* Genome-scale RNAi screen for host factors required for HIV replication. *Cell Host Microbe* **4**, 495-504 (2008).

27. Brass, A.L. *et al.* Identification of host proteins required for HIV infection through a functional genomic screen. *Science* **319**, 921-926 (2008).

28. Sorensen, M.G., Henriksen, K., Neutzsky-Wulff, A.V., Dziegiel, M.H. & Karsdal, M.A. Diphyllin, a novel and naturally potent V-ATPase inhibitor, abrogates acidification of the osteoclastic resorption lacunae and bone resorption. *J Bone Miner Res* **22**, 1640-1648 (2007).

29. Marsh, G.A., Hatami, R. & Palese, P. Specific residues of the influenza A virus hemagglutinin viral RNA are important for efficient packaging into budding virions. *J Virol* **81**, 9727-9736 (2007).

30. Chanda, S.K. *et al.* Genome-scale functional profiling of the mammalian AP-1 signaling pathway. *Proceedings of the National Academy of Sciences of the United States of America* **100**, 12153-12158 (2003).

31. Aza-Blanc, P. *et al.* Identification of modulators of TRAIL-induced apoptosis via RNAi-based phenotypic screening. *Molecular cell* **12**, 627-637 (2003).

32. Konig, R. *et al.* A probability-based approach for the analysis of large-scale RNAi screens. *Nat Methods* **4**, 847-849 (2007).

33. Goto, H. & Kawaoka, Y. A novel mechanism for the acquisition of virulence by a human influenza A virus. *Proc Natl Acad Sci U S A* **95**, 10224-10228 (1998).

34. Neumann, G., Hughes, M.T. & Kawaoka, Y. Influenza A virus NS2 protein mediates vRNP nuclear export through NES-independent interaction with hCRM1. *Embo J* **19**, 6751-6758 (2000).

35. Hui, E.K., Barman, S., Tang, D.H., France, B. & Nayak, D.P. YRKL sequence of influenza virus M1 functions as the L domain motif and interacts with VPS28 and Cdc42. *J Virol* **80**, 2291-2308 (2006).

36. Zhirnov, O.P., Ksenofontov, A.L., Kuzmina, S.G. & Klenk, H.D. Interaction of influenza A virus M1 matrix protein with caspases. *Biochemistry (Mosc)* **67**, 534-539 (2002).

37. LeBouder, F. *et al.* Annexin II incorporated into influenza virus particles supports virus replication by converting plasminogen into plasmin. *J Virol* **82**, 6820-6828 (2008).

38. Engelhardt, O.G., Smith, M. & Fodor, E. Association of the influenza A virus RNA-dependent RNA polymerase with cellular RNA polymerase II. *J Virol* **79**, 5812-5818 (2005).

39. Jorba, N. *et al.* Analysis of the interaction of influenza virus polymerase complex with human cell factors. *Proteomics* **8**, 2077-2088 (2008).

40. Kawaguchi, A. & Nagata, K. De novo replication of the influenza virus RNA genome is regulated by DNA replicative helicase, MCM. *Embo J* **26**, 4566-4575 (2007).

41. Melen, K. *et al.* Importin alpha nuclear localization signal binding sites for STAT1, STAT2, and influenza A virus nucleoprotein. *J Biol Chem* **278**, 28193-28200 (2003).

42. Gabriel, G., Herwig, A. & Klenk, H.D. Interaction of polymerase subunit PB2 and NP with importin alpha1 is a determinant of host range of influenza A virus. *PLoS Pathog* **4**, e11 (2008).

43. Tarendeau, F. *et al.* Structure and nuclear import function of the C-terminal domain of influenza virus polymerase PB2 subunit. *Nat Struct Mol Biol* **14**, 229-233 (2007).

44. O'Neill, R.E., Jaskunas, R., Blobel, G., Palese, P. & Moroianu, J. Nuclear import of influenza virus RNA can be mediated by viral nucleoprotein and transport factors required for protein import. *J Biol Chem* **270**, 22701-22704 (1995).

45. Deng, T. *et al.* Role of ran binding protein 5 in nuclear import and assembly of the influenza virus RNA polymerase complex. *J Virol* **80**, 11911-11919 (2006).

46. Furuta, Y. *et al.* Mechanism of action of T-705 against influenza virus. *Antimicrob Agents Chemother* **49**, 981-986 (2005).

47. Naito, T., Momose, F., Kawaguchi, A. & Nagata, K. Involvement of Hsp90 in assembly and nuclear import of influenza virus RNA polymerase subunits. *J Virol* **81**, 1339-1349 (2007).

48.   Hirayama, E., Atagi, H., Hiraki, A. & Kim, J. Heat shock protein 70 is related to thermal inhibition of nuclear export of the influenza virus ribonucleoprotein complex. *J Virol* **78**, 1263-1270 (2004).

49.   Garcia-Robles, I., Akarsu, H., Muller, C.W., Ruigrok, R.W. & Baudin, F. Interaction of influenza virus proteins with nucleosomes. *Virology* **332**, 329-336 (2005).

50.   Zhirnov, O.P. & Klenk, H.D. Histones as a target for influenza virus matrix protein M1. *Virology* **235**, 302-310 (1997).

51.   Huarte, M., Sanz-Ezquerro, J.J., Roncal, F., Ortin, J. & Nieto, A. PA subunit from influenza virus polymerase complex interacts with a cellular protein with homology to a family of transcriptional activators. *J Virol* **75**, 8597-8604 (2001).

52.   Honda, A. Role of host protein Ebp1 in influenza virus growth: intracellular localization of Ebp1 in virus-infected and uninfected cells. *J Biotechnol* **133**, 208-212 (2008).

53.   Elton, D. *et al.* Interaction of the influenza virus nucleoprotein with the cellular CRM1-mediated nuclear export pathway. *J Virol* **75**, 408-419 (2001).

54.   Momose, F., Kikuchi, Y., Komase, K. & Morikawa, Y. Visualization of microtubule-mediated transport of influenza viral progeny ribonucleoprotein. *Microbes Infect* **9**, 1422-1433 (2007).

55.   Momose, F. *et al.* Identification of Hsp90 as a stimulatory host factor involved in influenza virus RNA synthesis. *J Biol Chem* **277**, 45306-45314 (2002).

56.   Shaw, M.L., Stone, K.L., Colangelo, C.M., Gulcicek, E.E. & Palese, P. Cellular proteins in influenza virus particles. *PLoS Pathog* **4**, e1000085 (2008).

57.   Digard, P. *et al.* Modulation of nuclear localization of the influenza virus nucleoprotein through interaction with actin filaments. *J Virol* **73**, 2222-2231 (1999).

58.   Mayer, D. *et al.* Identification of cellular interaction partners of the influenza virus ribonucleoprotein complex and polymerase complex using proteomic-based approaches. *J Proteome Res* **6**, 672-682 (2007).

59.   Mibayashi, M. *et al.* Inhibition of retinoic acid-inducible gene I-mediated induction of beta interferon by the NS1 protein of influenza A virus. *J Virol* **81**, 514-524 (2007).

60.   Pichlmair, A. *et al.* RIG-I-mediated antiviral responses to single-stranded RNA bearing 5'-phosphates. *Science* **314**, 997-1001 (2006).

61.   Li, S., Min, J.Y., Krug, R.M. & Sen, G.C. Binding of the influenza A virus NS1 protein to PKR mediates the inhibition of its activation by either PACT or double-stranded RNA. *Virology* **349**, 13-21 (2006).

62.   Hale, B.G., Jackson, D., Chen, Y.H., Lamb, R.A. & Randall, R.E. Influenza A virus NS1 protein binds p85beta and activates phosphatidylinositol-3-kinase signaling. *Proc Natl Acad Sci U S A* **103**, 14194-14199 (2006).

63.   Murayama, R. *et al.* Influenza A virus non-structural protein 1 (NS1) interacts with cellular multifunctional protein nucleolin during infection. *Biochem Biophys Res Commun* **362**, 880-885 (2007).

64.   Wolff, T., O'Neill, R.E. & Palese, P. NS1-Binding protein (NS1-BP): a novel human protein that interacts with the influenza A virus nonstructural NS1 protein is relocalized in the nuclei of infected cells. *J Virol* **72**, 7170-7180 (1998).

65.   Falcon, A.M., Fortes, P., Marion, R.M., Beloso, A. & Ortin, J. Interaction of influenza virus NS1 protein and the human homologue of Staufen in vivo and in vitro. *Nucleic Acids Res* **27**, 2241-2247 (1999).

66.   Burgui, I., Aragon, T., Ortin, J. & Nieto, A. PABP1 and eIF4GI associate with influenza virus NS1 protein in viral mRNA translation initiation complexes. *J Gen Virol* **84**, 3263-3274 (2003).

67.   Satterly, N. *et al.* Influenza virus targets the mRNA export machinery and the nuclear pore complex. *Proc Natl Acad Sci U S A* **104**, 1853-1858 (2007).

68. Kochs, G., Garcia-Sastre, A. & Martinez-Sobrido, L. Multiple anti-interferon actions of the influenza A virus NS1 protein. *J Virol* **81**, 7011-7021 (2007).

69. Noah, D.L., Twu, K.Y. & Krug, R.M. Cellular antiviral responses against influenza A virus are countered at the posttranscriptional level by the viral NS1A protein via its binding to a cellular protein required for the 3' end processing of cellular pre-mRNAS. *Virology* **307**, 386-395 (2003).

70. Nemeroff, M.E., Barabino, S.M., Li, Y., Keller, W. & Krug, R.M. Influenza virus NS1 protein interacts with the cellular 30 kDa subunit of CPSF and inhibits 3'end formation of cellular pre-mRNAs. *Mol Cell* **1**, 991-1000 (1998).

71. Zamarin, D., Garcia-Sastre, A., Xiao, X., Wang, R. & Palese, P. Influenza virus PB1-F2 protein induces cell death through mitochondrial ANT3 and VDAC1. *PLoS Pathog* **1**, e4 (2005).

72. Marjuki, H. *et al.* Higher polymerase activity of a human influenza virus enhances activation of the hemagglutinin-induced Raf/MEK/ERK signal cascade. *Virol J* **4**, 134 (2007).

73. Zhou, Y. *et al.* In silico gene function prediction using ontology-based pattern identification. *Bioinformatics (Oxford, England)* **21**, 1237-1245 (2005).

74. Young, J.A. *et al.* The Plasmodium falciparum sexual development transcriptome: a microarray analysis using ontology-based pattern identification. *Molecular and biochemical parasitology* **143**, 67-79 (2005).

75. Rines, D.R. *et al.* Whole genome functional analysis identifies novel components required for mitotic spindle integrity in human cells. *Genome Biol* **9**, R44 (2008).

76. Stertz, S. *et al.* The antiviral potential of interferon-induced cotton rat Mx proteins against orthomyxovirus (influenza), rhabdovirus, and bunyavirus. *J Interferon Cytokine Res* **27**, 847-855 (2007).

77. O'Neill, R.E., Talon, J. & Palese, P. The influenza virus NEP (NS2 protein) mediates the nuclear export of viral ribonucleoproteins. *EMBO J* **17**, 288-296 (1998).

78. Hoffmann, H.H., Palese, P. & Shaw, M.L. Modulation of influenza virus replication by alteration of sodium ion transport and protein kinase C activity. *Antiviral Res* **80**, 124-134 (2008).

79. Donelan, N.R., Basler, C.F. & Garcia-Sastre, A. A recombinant influenza A virus expressing an RNA-binding-defective NS1 protein induces high levels of beta interferon and is attenuated in mice. *J Virol* **77**, 13257-13266 (2003).

80. Park, M.S. *et al.* Newcastle disease virus (NDV)-based assay demonstrates interferon-antagonist activity for the NDV V protein and the Nipah virus V, W, and C proteins. *J Virol* **77**, 1501-1511 (2003).
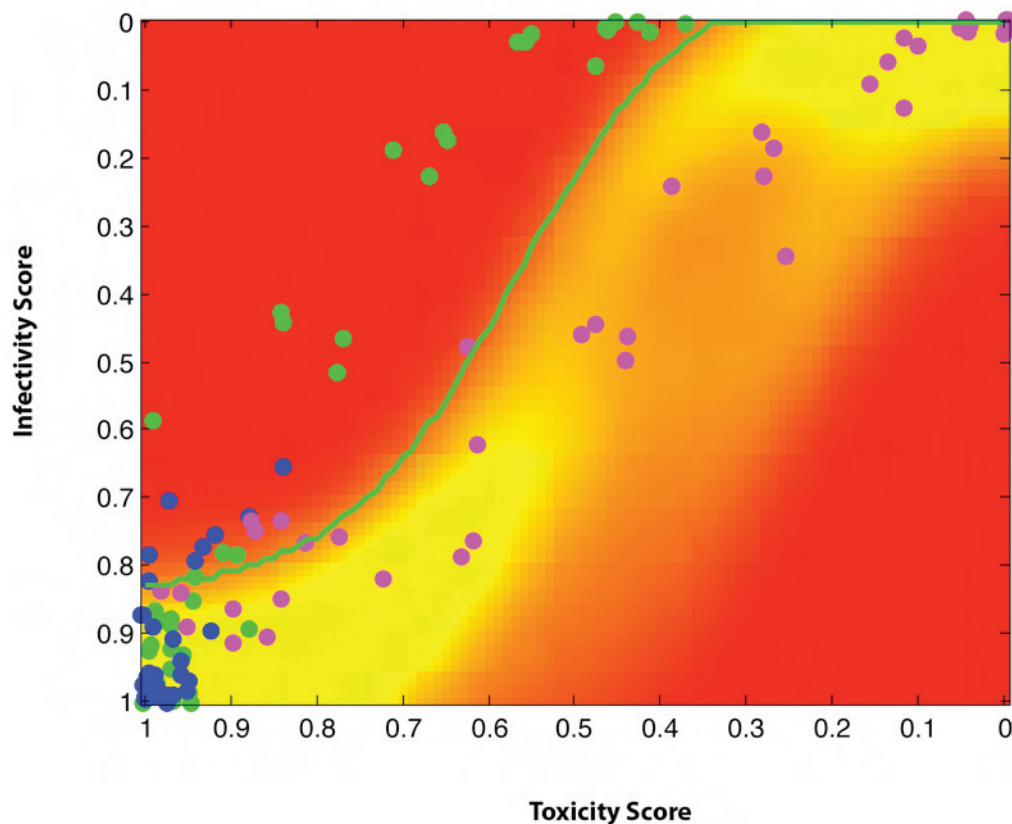
Figure S1. Infectivity - toxicity relationship curve. To establish a threshold for discarding siRNAs that induce cellular toxicity, we investigated the impact of a dilution series (right to left on X-axis) of a toxic siRNA (siRPS27A- pink circles), an siRNA known to inhibit influenza virus Renilla luciferase reporter activity (siRNA targeting Renilla- green circles), and a negative control siRNA (blue circle) on both influenza A virus replication and cellular toxicity assay. A score of zero represents low virus replication or reduced cell viability and a score of one represents maximum activity in corresponding assays. For example, the lowest dilution of positive control siRNAs scores 1 in the infectivity score (bottom left), and the highest dilution scores 0 (top). The toxicity score for each of these are 1 and 0.4, respectively. Based on these relationships, a decision boundary was established (green curve; see methods); if an siRNA fell below the boundary, it was considered to be toxic. Otherwise, it was considered a true hit (p<0.05). Three siRNAs were tested in ≥4 replicates. Toxic control (pink circles) fell below the decision boundary. Positive control (green circles) fell above the decision boundary. Negative non-toxic control (blue circles) mostly fell below the decision boundary.
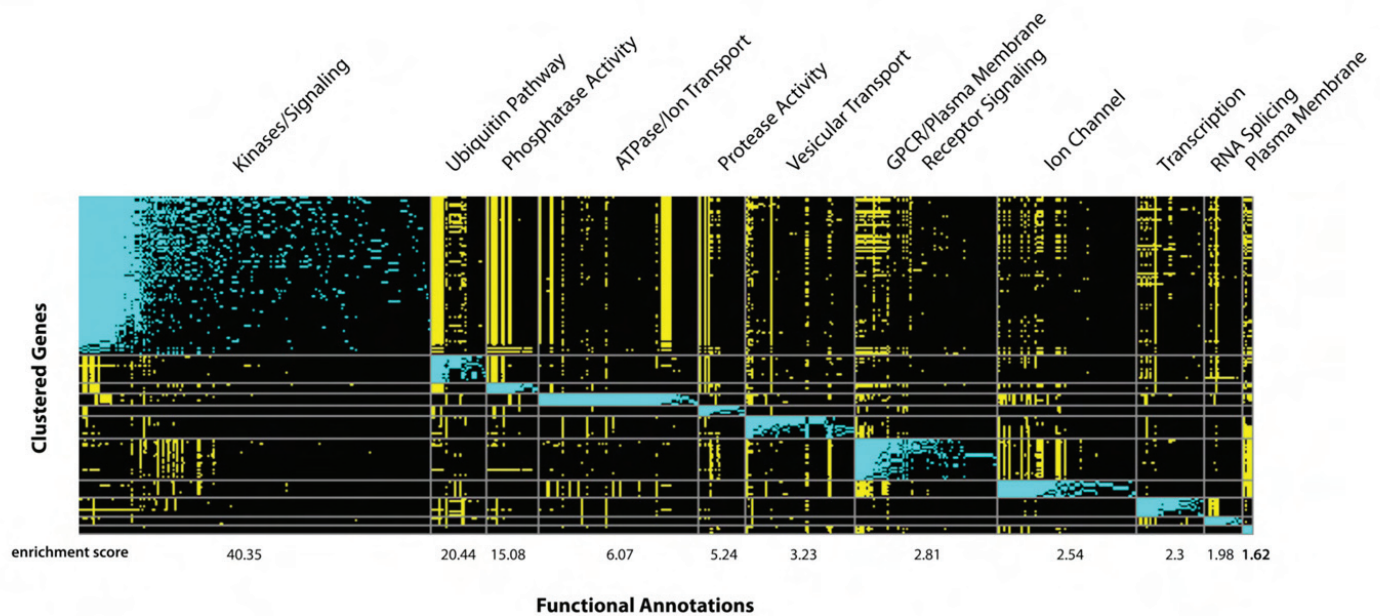
Figure S2. Functional classification of influenza A virus-host cellular proteins. 177 of the 295 identified host proteins were classified into related functional groups revealing 11 highly overrepresented biological processes required for influenza virus replication. Host cellular genes are represented on the y-axis, and their inclusion in a primary functional category (blue) or secondary function category (yellow) is indicated along the x-axis. Boundaries of gene clusters and biological processes are represented by gray lines. Enrichment scores for each functional class are also given. Functional classification and enrichment analysis was conducted using the Database for Annotation, Visualization and Integrated Discovery (DAVID) Bioinformatics Resource[10].
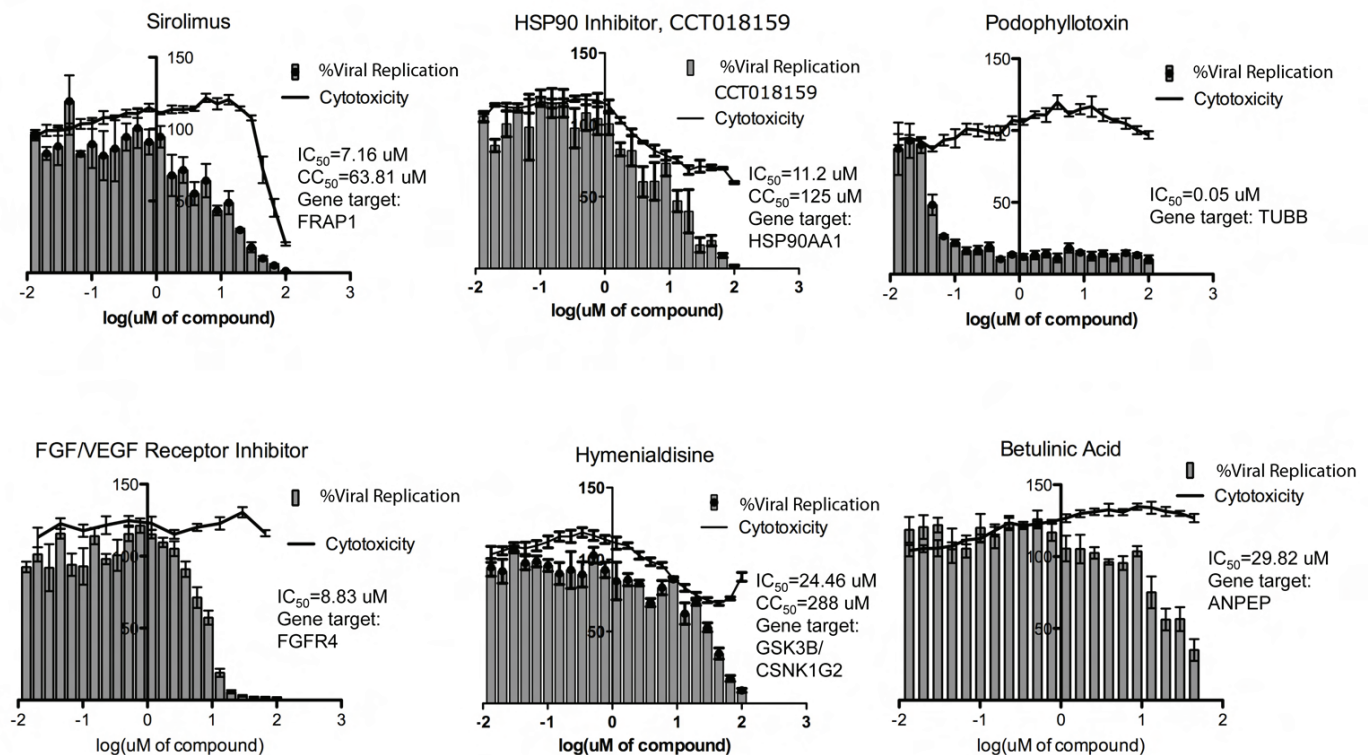
Figure S3. Small molecule inhibitors targeting identified host factors reduce influenza virus growth. MDCK-HA cells were infected with WSN-Ren virus at an MOI of 0.03 in the presence of increasing concentrations of various inhibitors targeting specific host genes that were confirmed as host cellular factors for influenza virus entry. DMSO control was set to a 100%. Virus growth was assayed at 36 h post-infection and mean inhibition +/- standard deviation of triplicate samples are shown as grey bars. The concentrations for 50% inhibition (IC_{50}) and the respective target genes are indicated. Cell viability (toxicity) with increasing concentrations of each respective inhibitor was assessed in parallel experiments (black lines). Small molecules targeting host factors are as follows: Sirolimus (Rapamycin) and FRAP1 (mTOR; GeneID 2475)[11-13]; HSP90 Inhibitor CCT018159 (4-(4-(2,3-Dihydro-1,4-benzodioxin-6-yl)-5-methyl-1H-pyrazol-3-yl)-6-ethylresorcinol) and HSP90AA1 (GeneID 3320)[14-16]; Podophyllotoxin (Podophyllinic Acid Lactone) and TUBB (tubulin beta; Gene ID 203068)[17]; FGF/VEGF Receptor Inhibitor (4-Hydroxy-3-benzimidazol-2-ylhydroquinolin-2-one) and FGFR4 (GeneID 2264; possibly also FGFR2 (GeneID 2263), or VEGFB (GeneID 7423)[18]; Hymenialdisine and GSK3b (GeneID 2932)[19, 20]; and Betulinic Acid and ANPEP (aminopeptidase N; GeneID 290)[21]. Inhibition of HSP90 has been recently shown to inhibit influenza virus replication[22].

Supplemental Figure S4
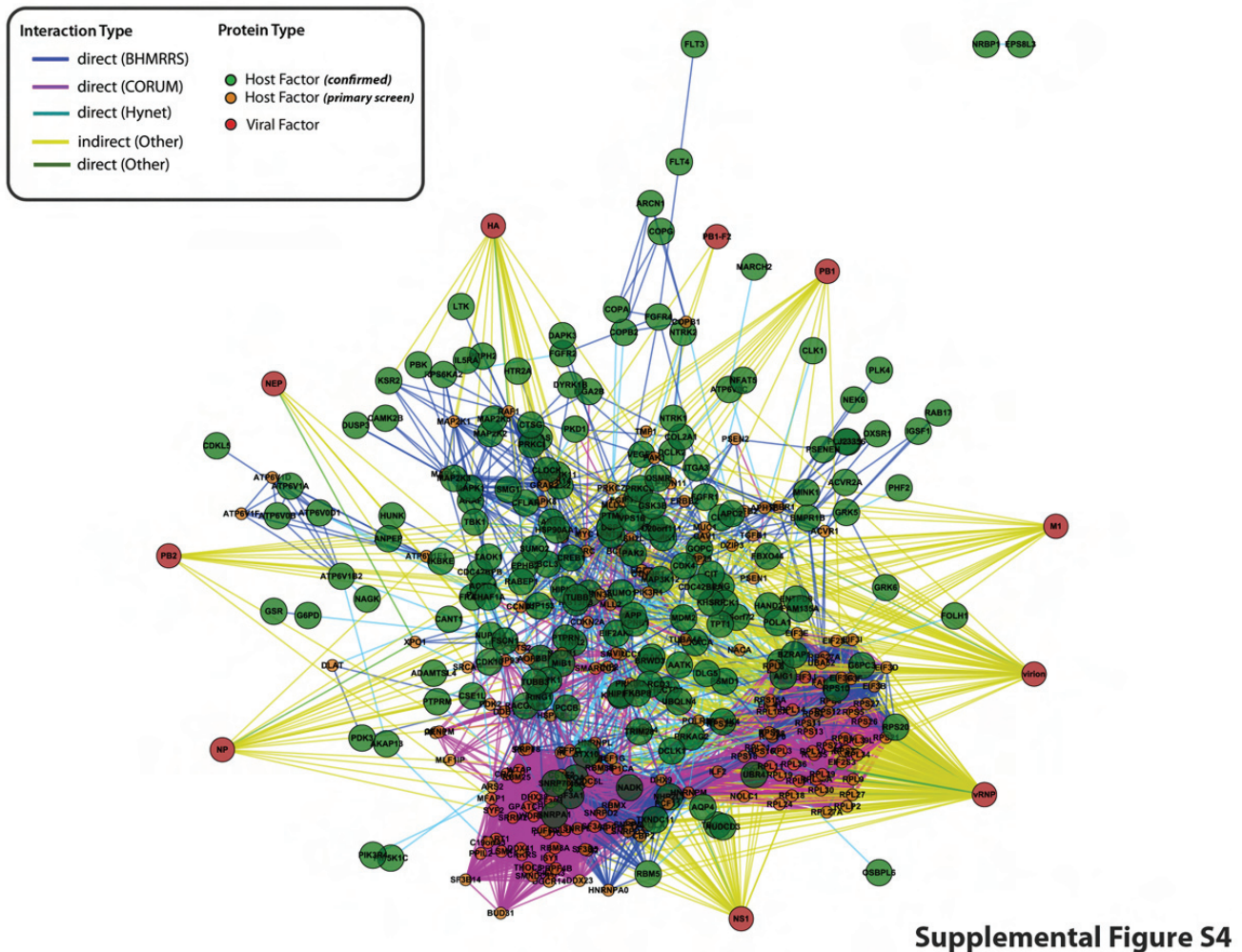
Figure S4. Influenza host-pathogen interaction map. This is an enlarged representation of Figure 1C with protein annotations. Binary protein interaction data is listed in Supplemental Table S6. Interaction data was elucidated based on binary protein interaction data derived from publically available databases including BIND, HPRD, MINT, Reactome, Rual et al.[23], and Stelzl et al. [24] (BHMRRS; blue connections), curated protein complex data (CORUM; pink connections), the Hynet yeast two-hybrid database (aqua connections), and published viral-protein interaction data (see materials and methods; yellow and green connections). Red circles indicate influenza nodes, while green circles represent confirmed factors, and orange circles indicate unconfirmed influenza host proteins identified in the primary RNAi screen. Viral nodes were abbreviated as follows: HA (Hemagglutinin), NS1 (NS1 protein), M1 (M1 Matrix protein), NEP (NEP/NS2 protein), NP (NP protein), PB1 and PB2 (the polymerase subunits PB1 and PB2), PB1-F2 (PB1-F2 protein), vRNP (influenza viral ribonucleoprotein complex), virion (proteins incorporated into virions).

Supplemental Figure 5a
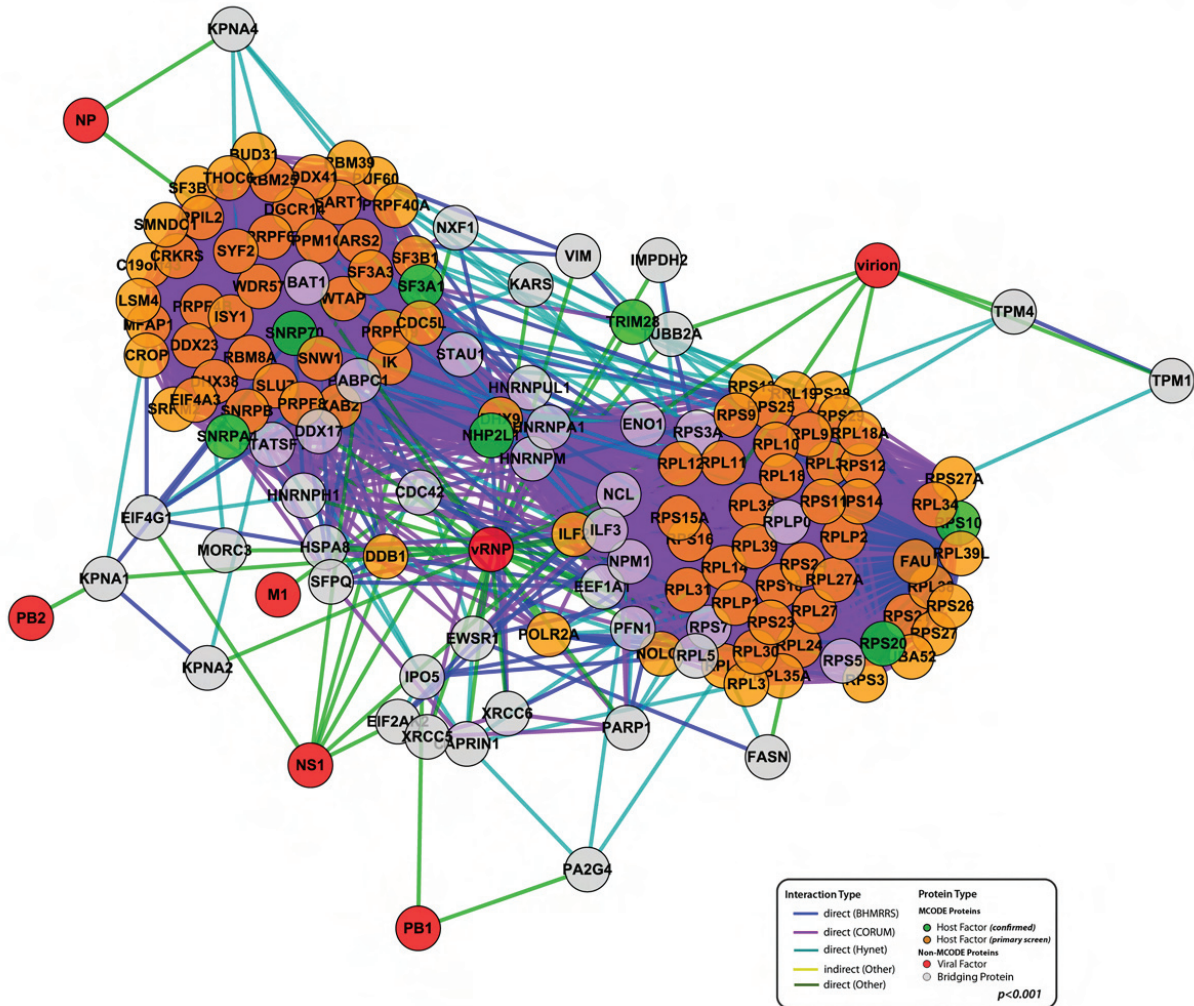
Supplemental Figure 5b
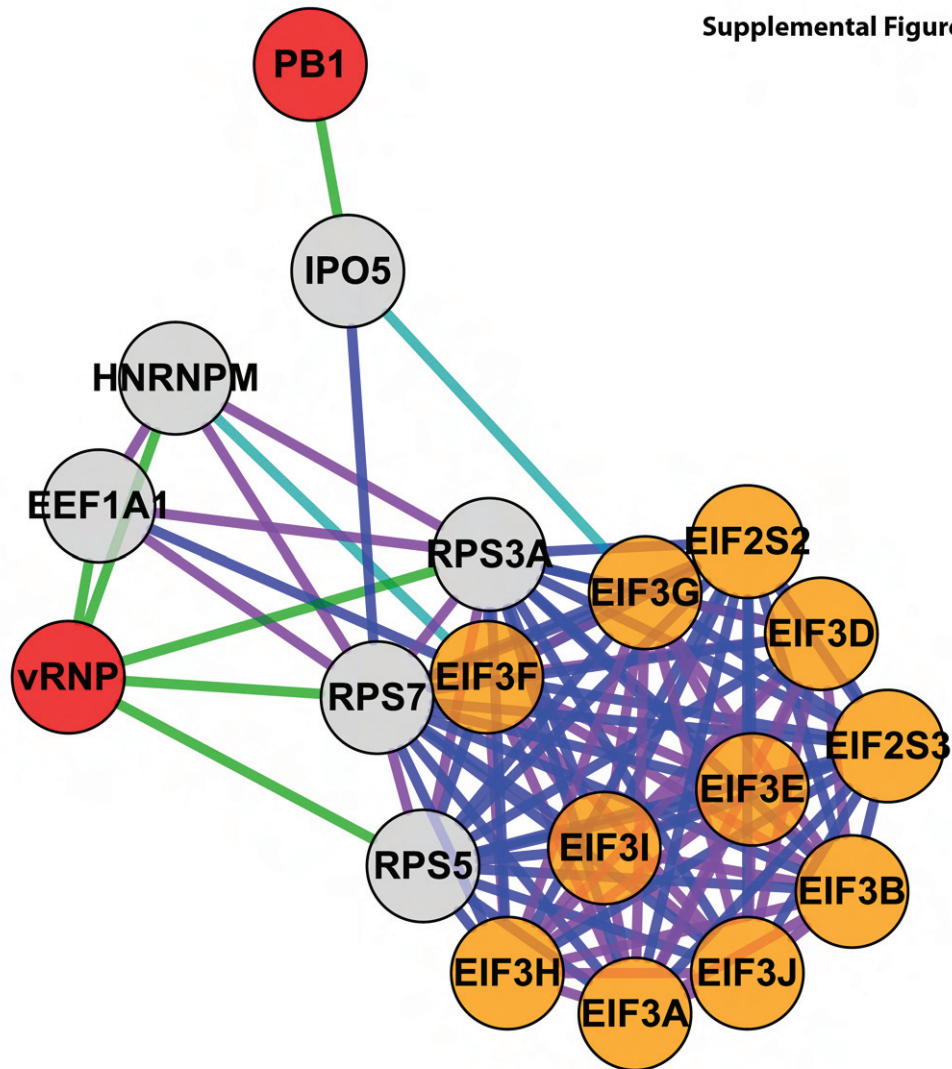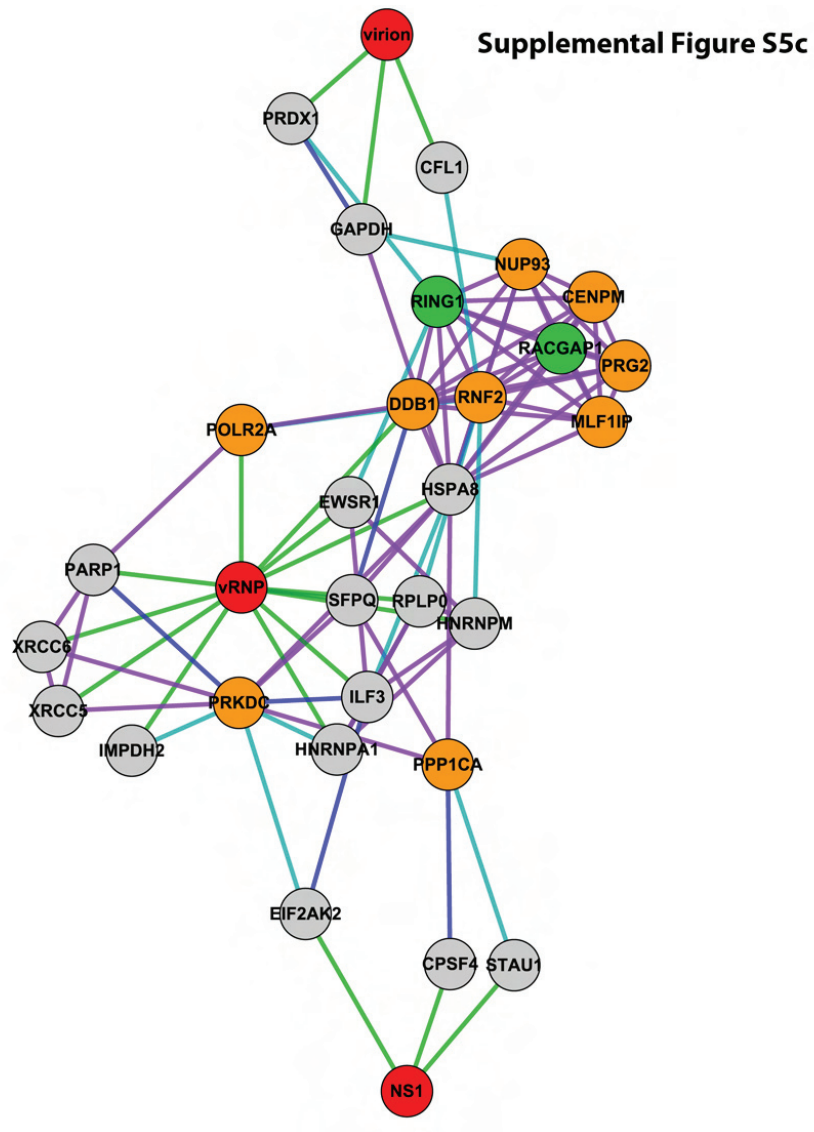
Supplemental Figure S5c
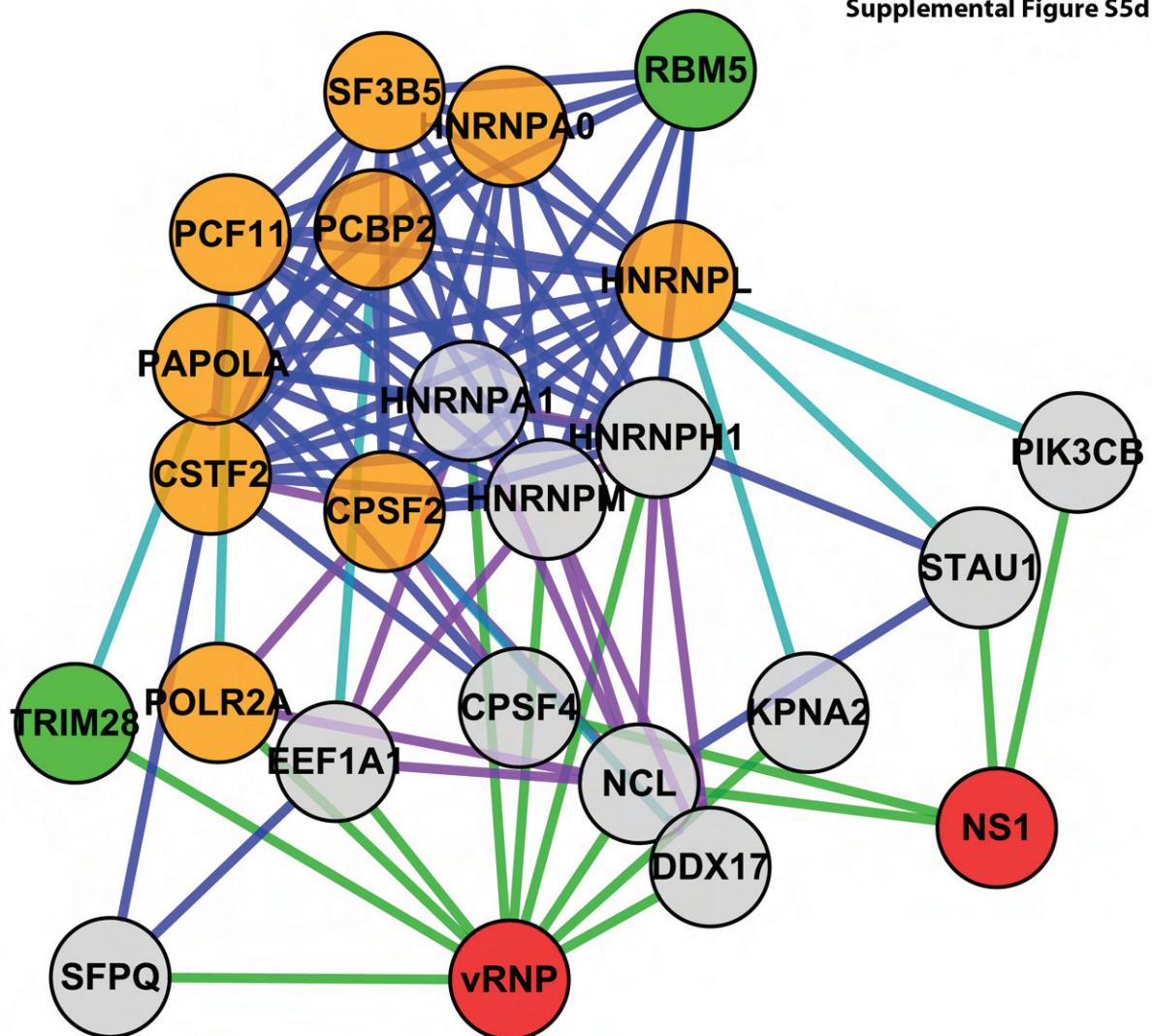
Supplemental Figure S5e
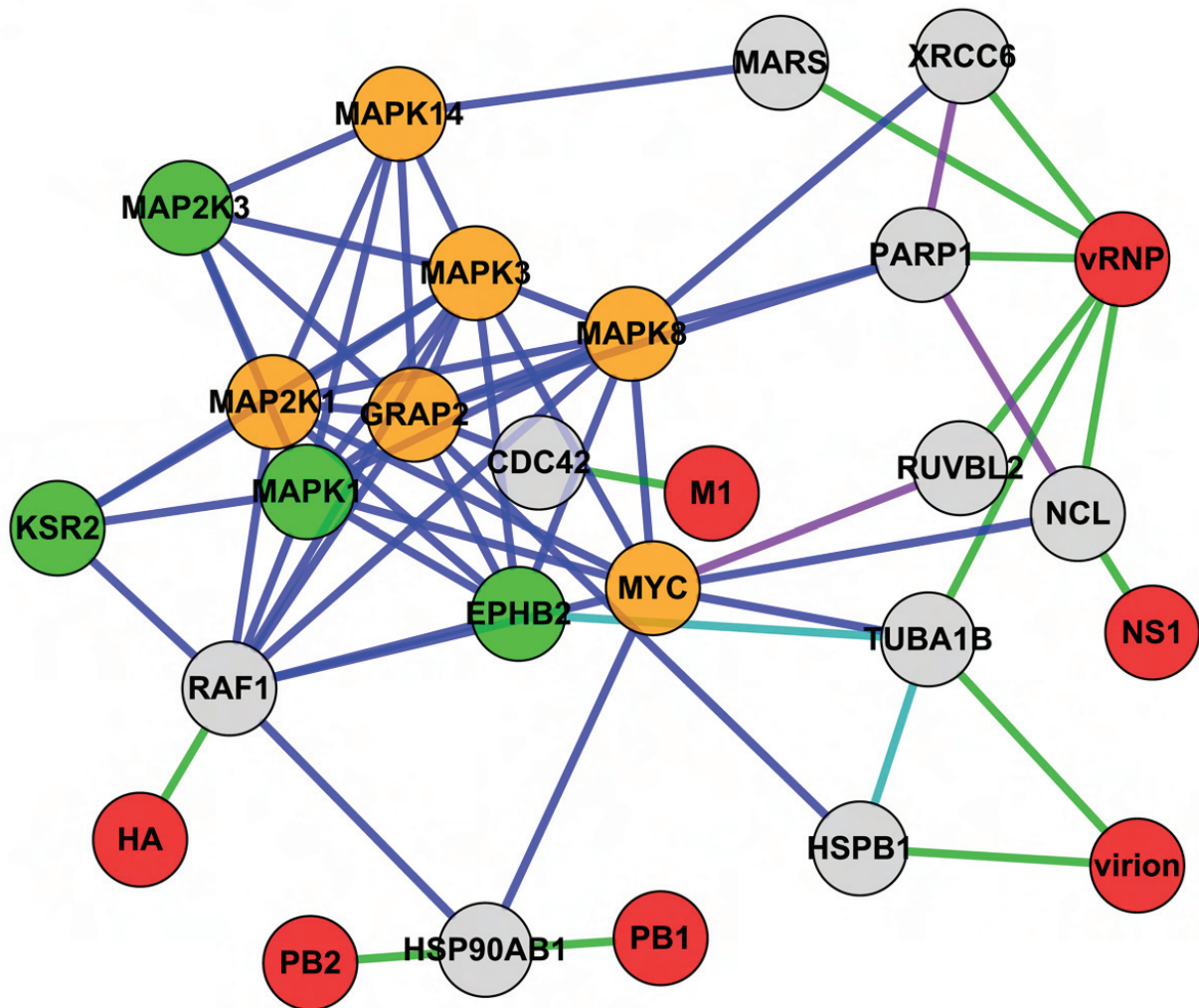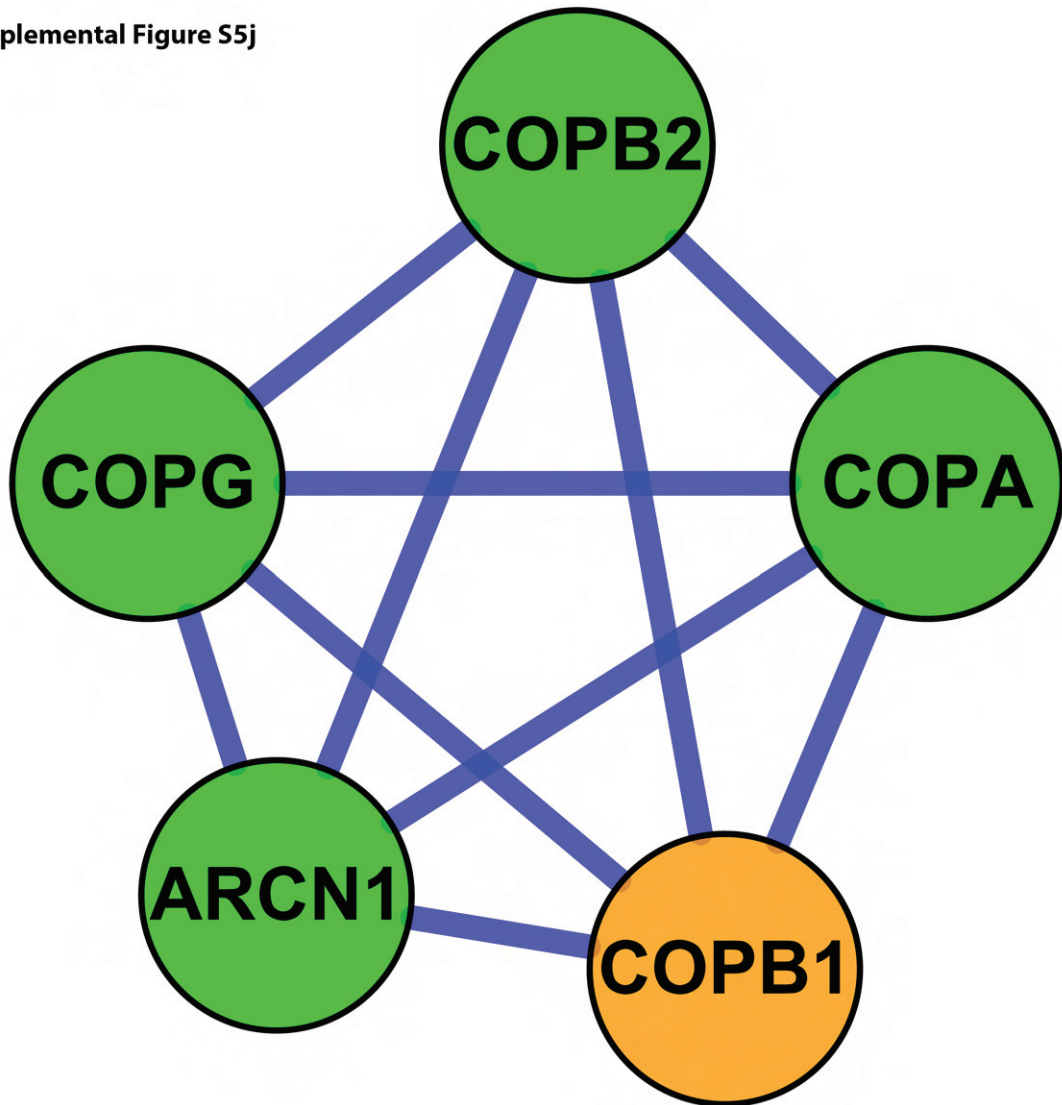
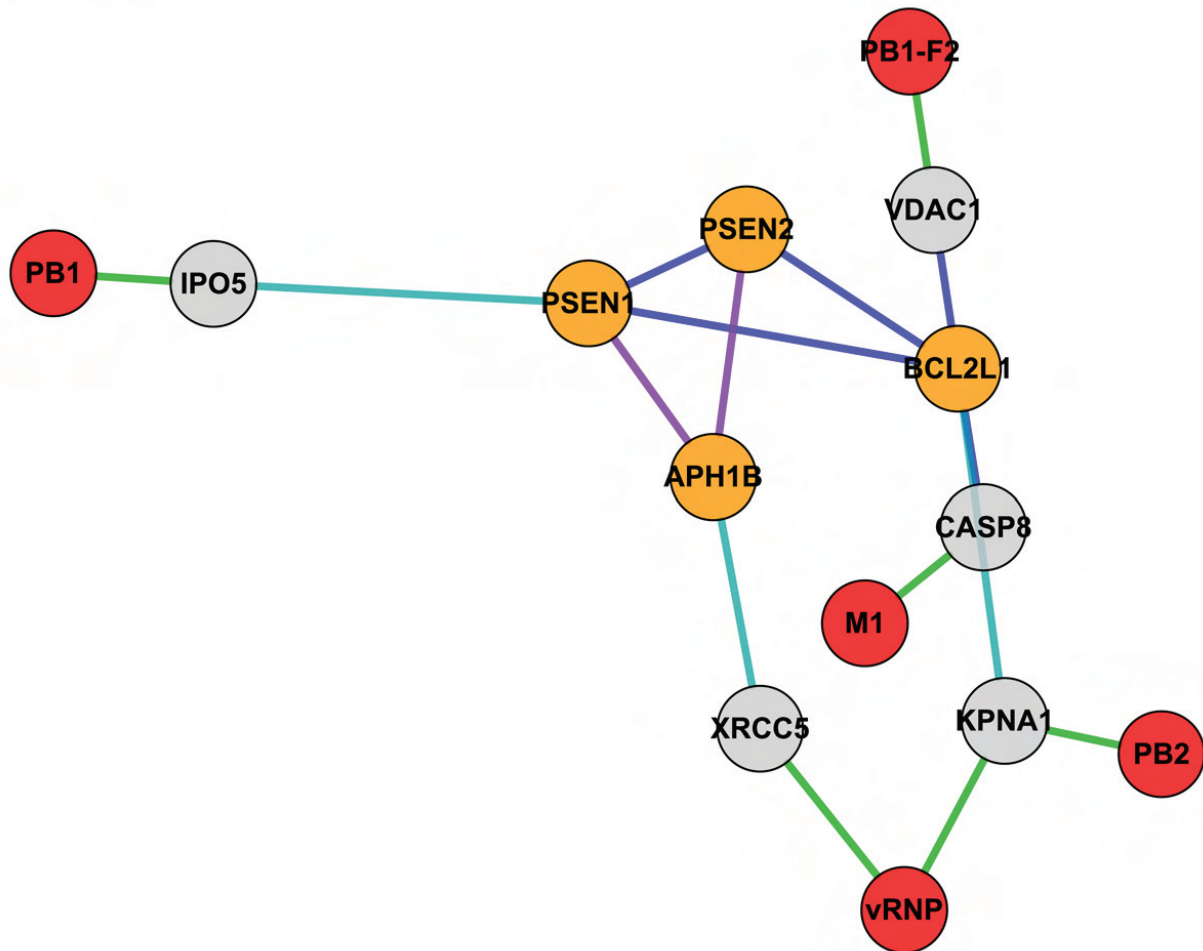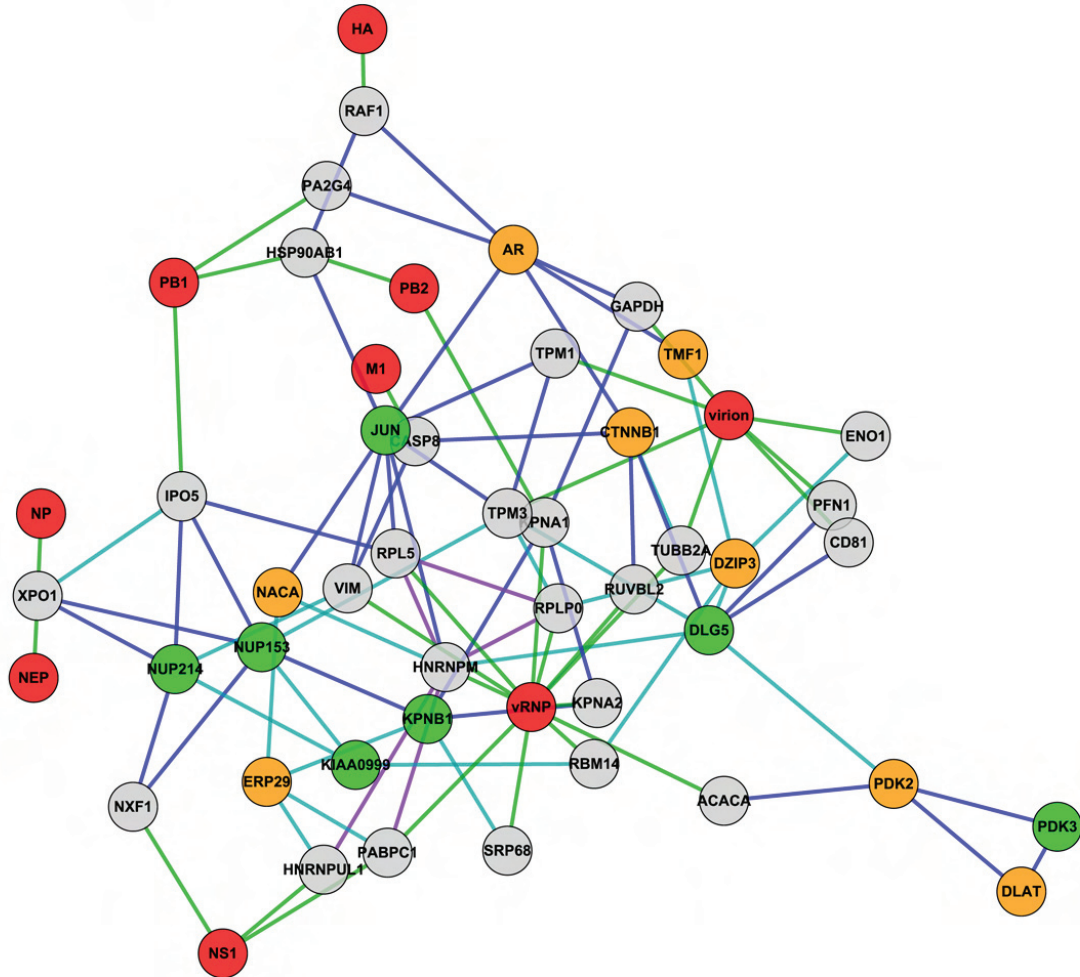Supplemental Figure S5f
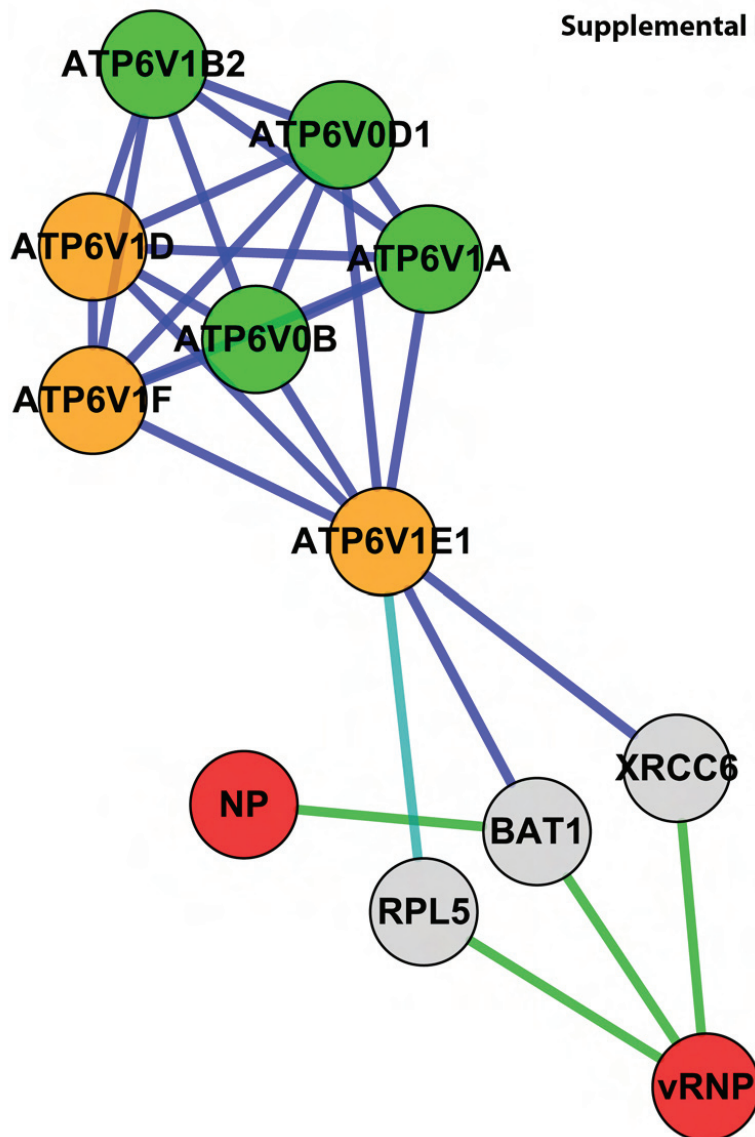
Supplemental Figure S5g
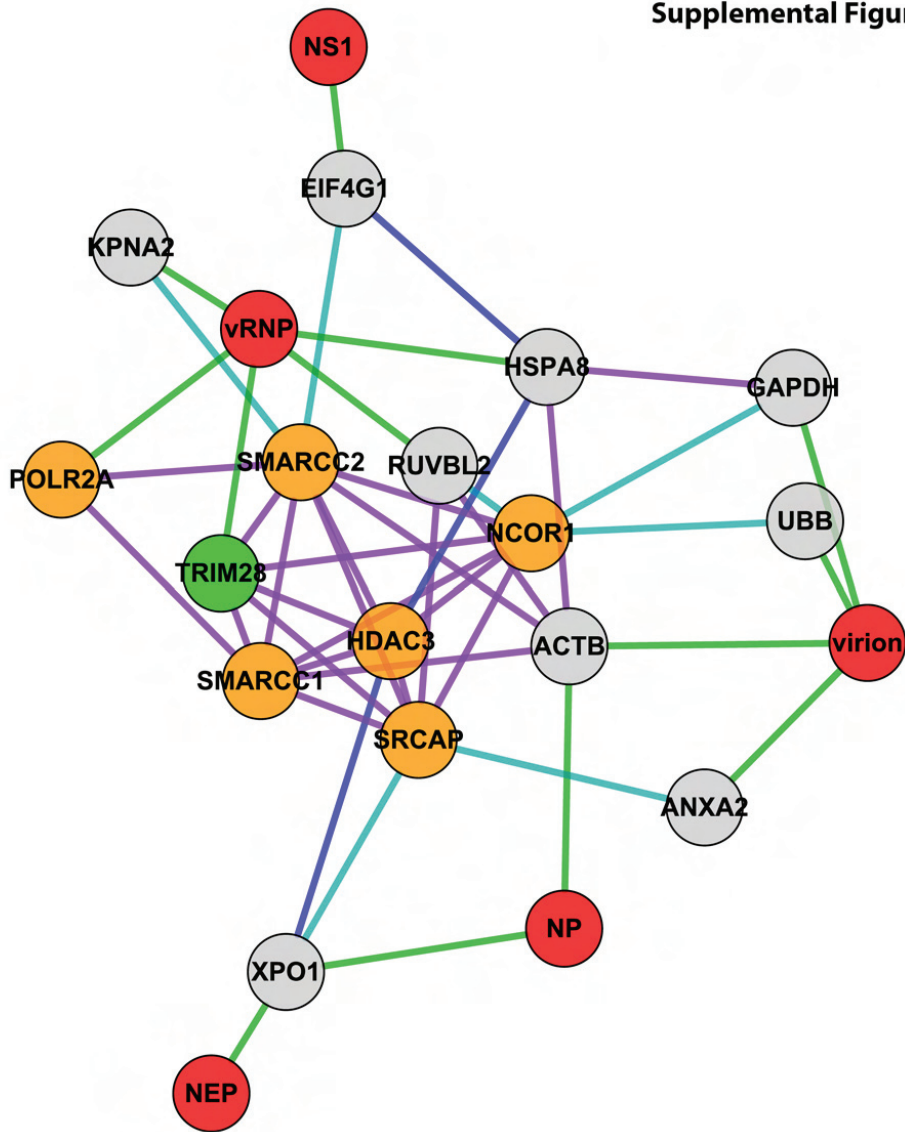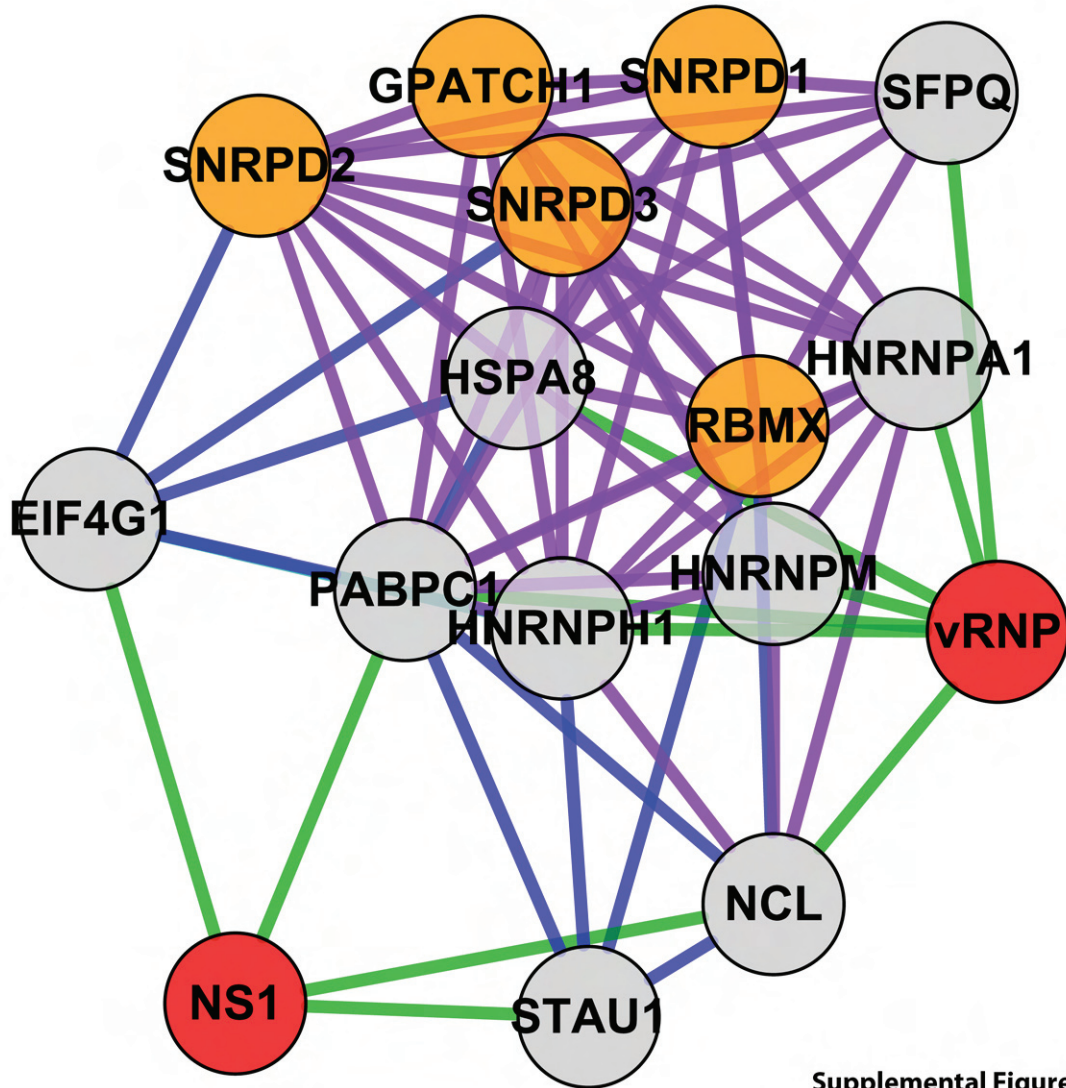
Supplemental Figure S5h

Supplemental Figure S5i
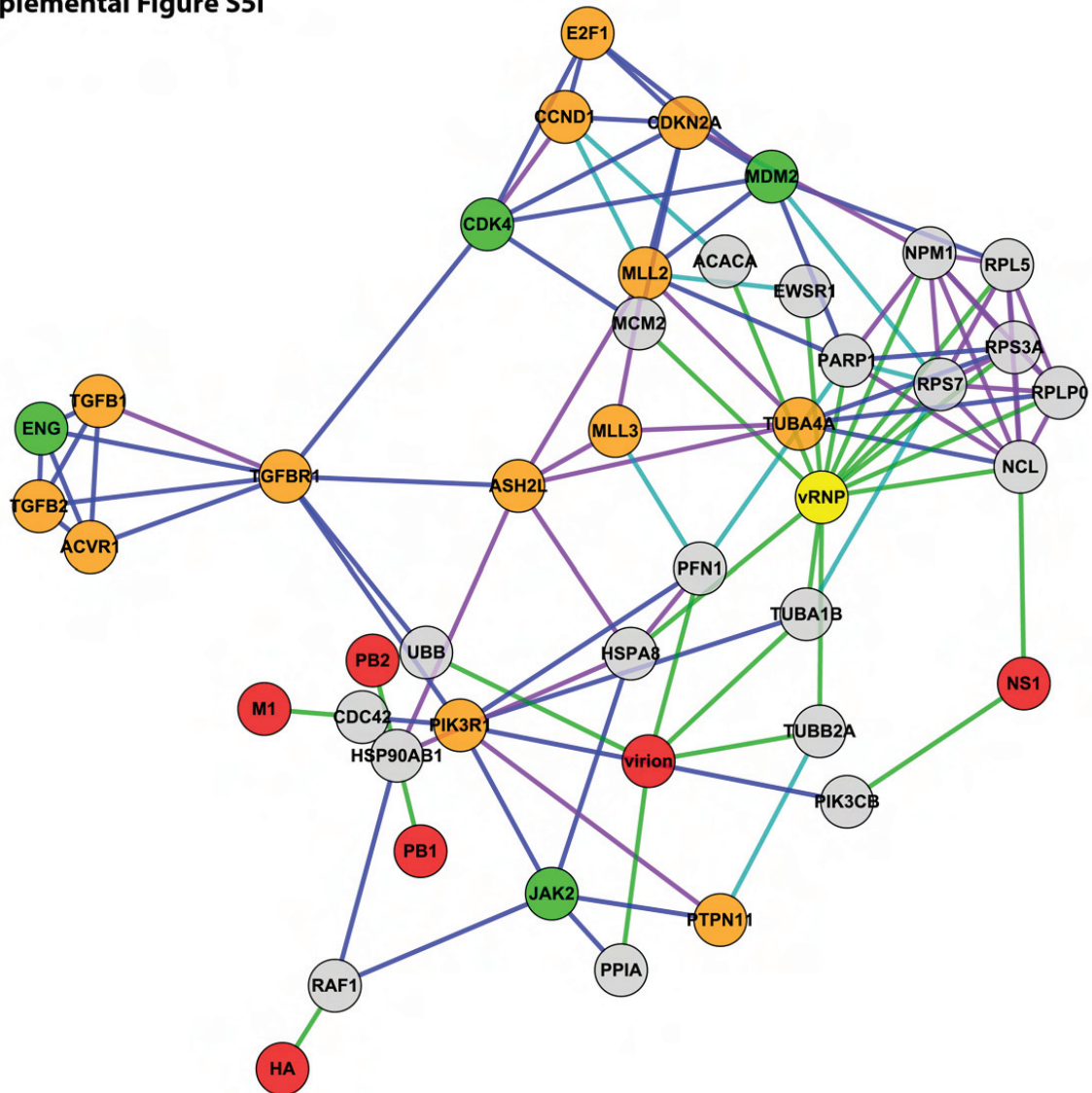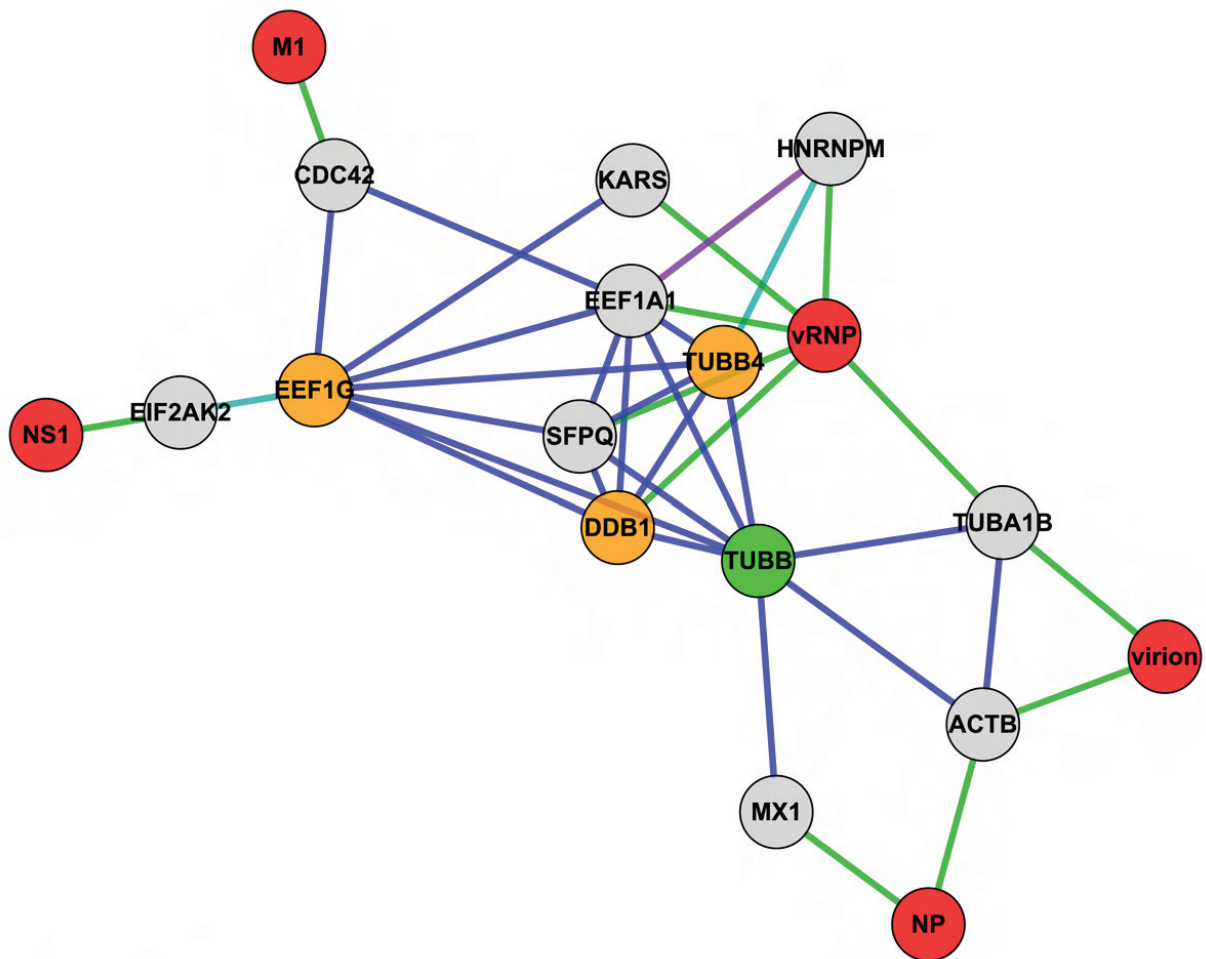
Supplemental Figure S5j

Supplemental Figure S5k

Supplemental S5l

Supplemental Figure S5m

Supplemental Figure S5n

Supplemental Figure 5o
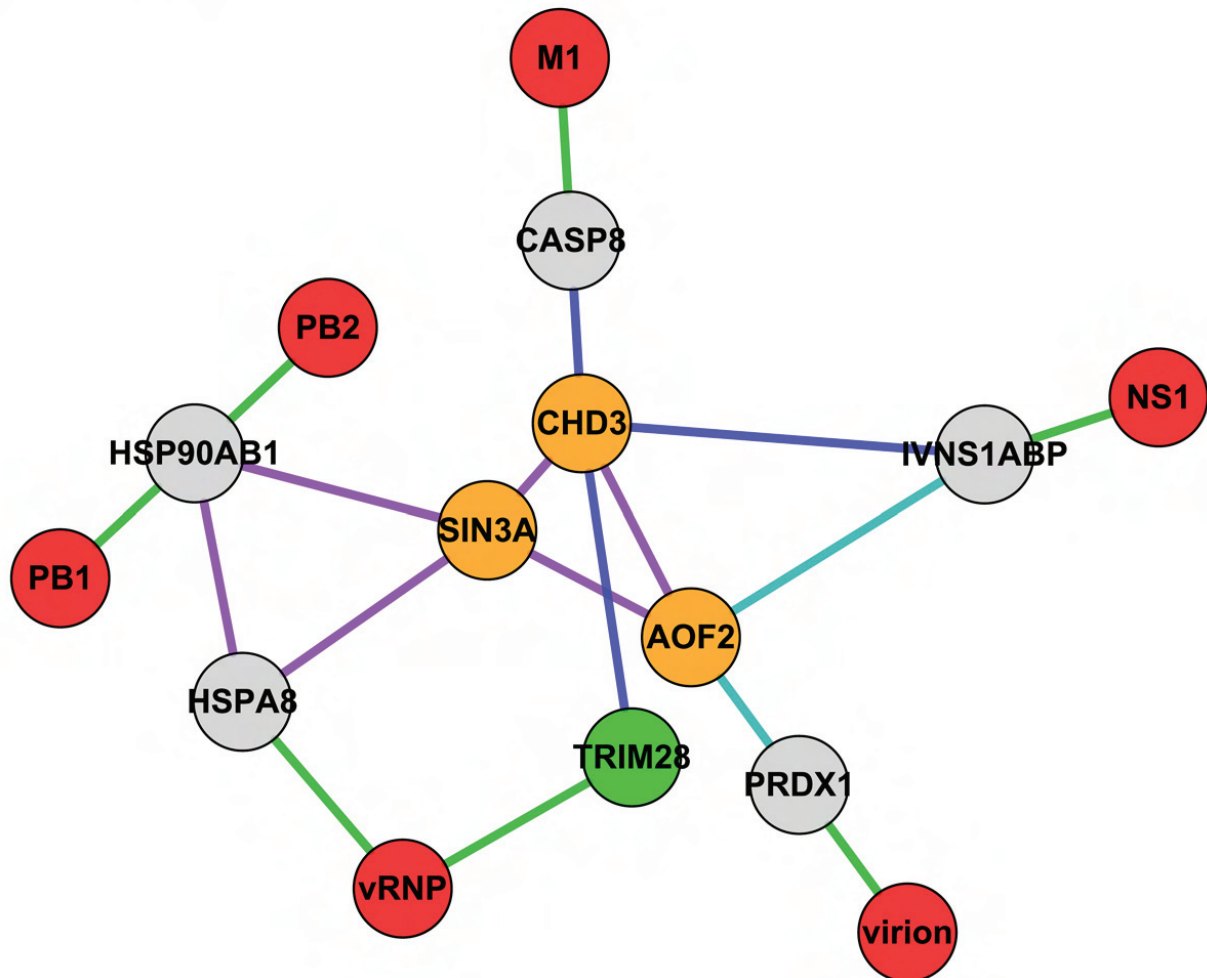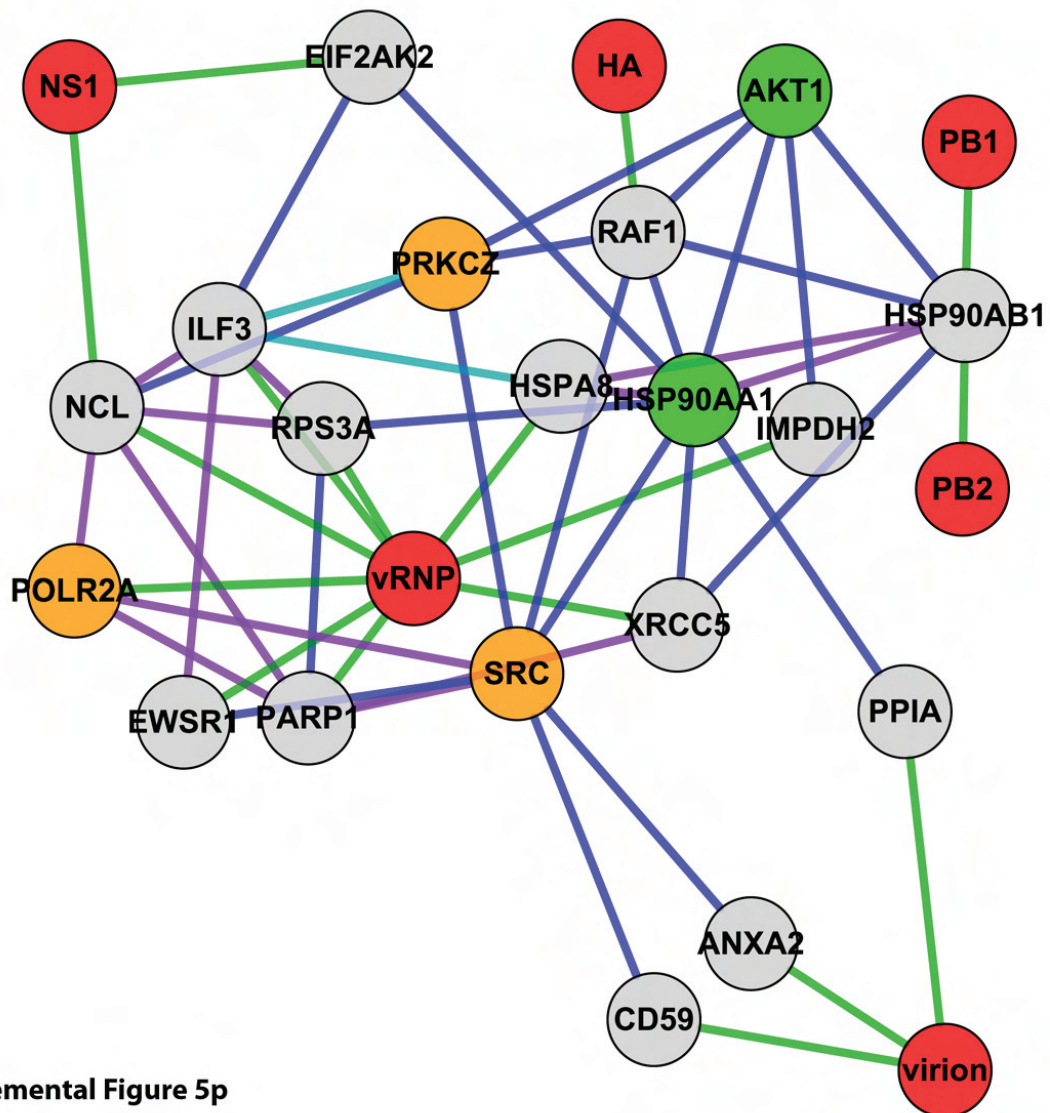
Supplemental Figure 5p
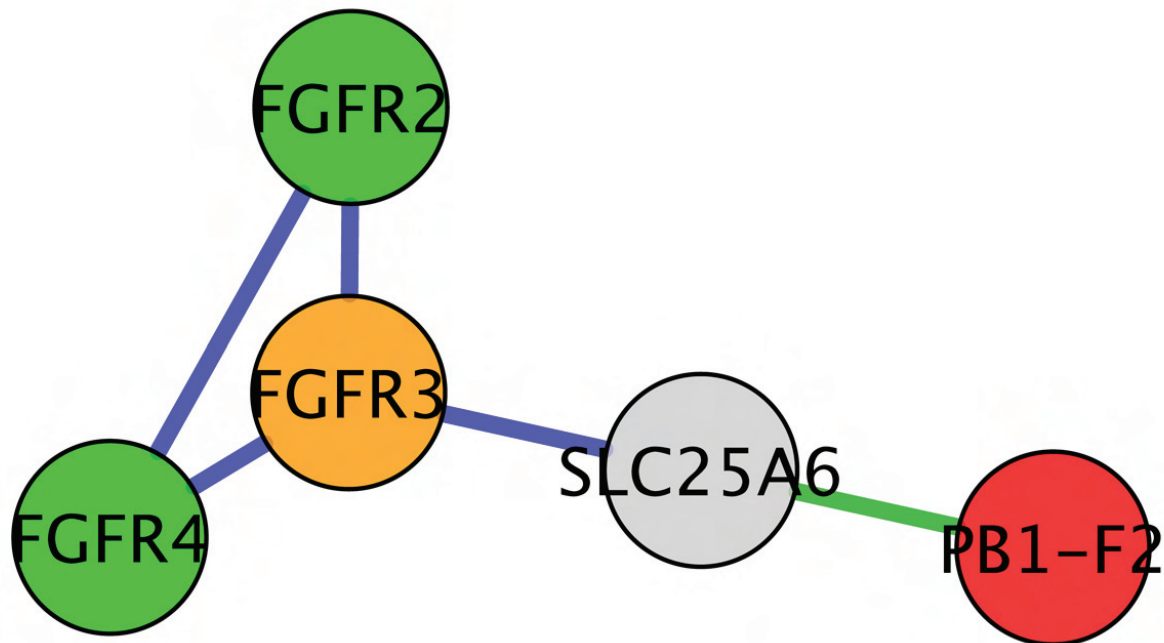
Supplemental Figure 5q

Figure S5. Analysis of biochemical clusters that constitute the influenza virus-host interaction network. To identify locally dense protein neighborhoods likely to reflect endogenous protein complexes, MCODE analysis[25] was conducted on the network shown in Figure 1c. We highlight the following complexes: RNA binding and splicing (S5a), translation (S5b), DNA repair and recombination (S5c), RNA splicing (S5d), MAPK signaling (S5e), v-ATPases (S5f), transcription (S5g), spliceosome components (S5h), cell cycle (S5i), COPI (j), signal transduction (S5k), Notch signaling (S5l), nuclear import/signaling (S5m), cytoskeleton (S5n), chromatin (S5o), and PKC signaling (S5p), and FGFR signaling (S5q). Interaction data was elucidated based on binary protein interaction data derived from publically available databases including BIND, HPRD, MINT, Reactome, Rual et al.[23], and Stelzl et al. [24] (BHMRRS; blue connections), curated protein complex data (CORUM; pink connections), the Hynet yeast two-hybrid database (aqua connections), and published viral-protein interaction data (see materials and methods; yellow and green connections). MCODE cluster proteins are shown in green, which represent confirmed factors, and orange, which indicate unconfirmed influenza-host proteins identified in the primary RNAi screen. Non-MCODE proteins are reflected by red circles, indicating influenza nodes, while grey circles are "bridging" proteins that facilitate (indirect) interactions between influenza virus proteins and the identified host factors.
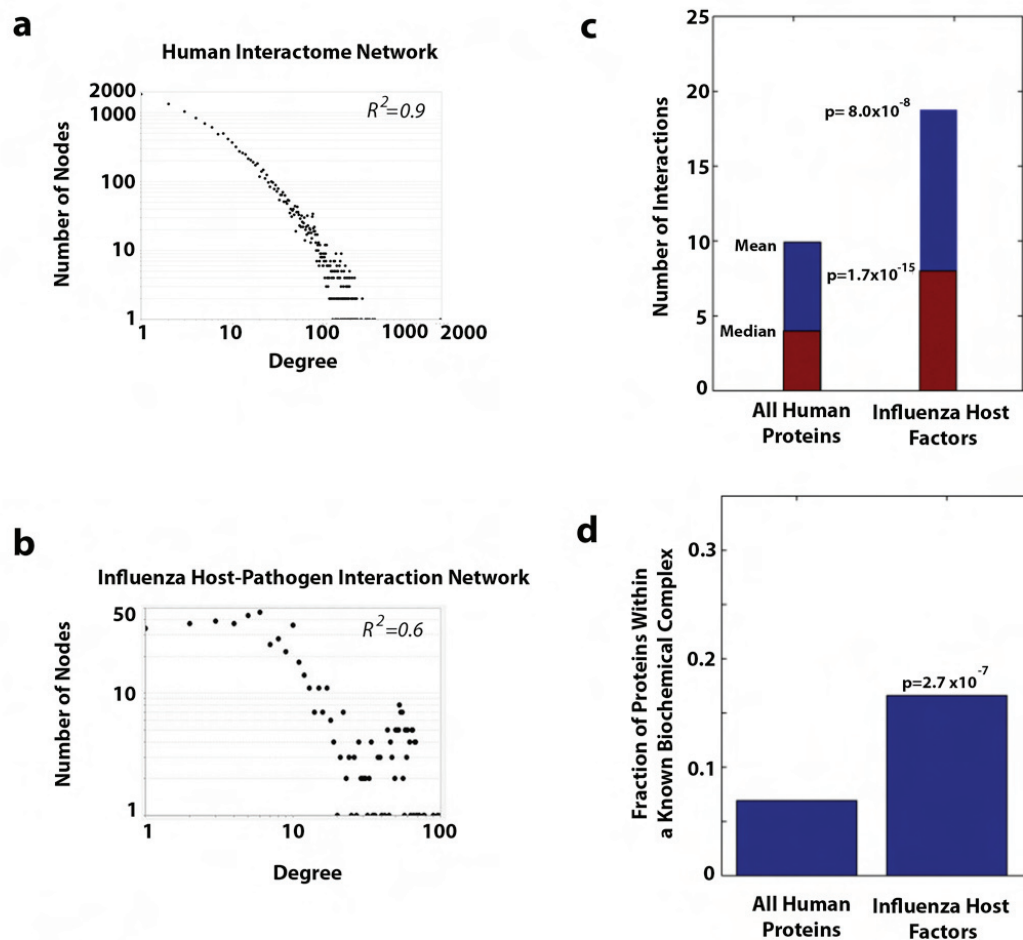
Figure S6. Power law distribution and enrichment of hubs and higher-order complexes amongst influenza virus-host cellular factors. (a) Node degree distributions of the human interactome network used in this study (see methods) follow a power-law distribution (R^2=0.9), indicating that this dataset reflects an unbiased real world ("scale-free") network. (b) The influenza host-pathogen interaction network also resembles a scale-free network (R^2=0.6), although not to the extent of the human interactome network due to its limited size. (c) We computed the mean and median number of interactions (node degrees) for all proteins found in the described human interactome databases, and those identified to be required for influenza virus replication by RNAi analysis. Significance (p values) is shown. The two-tailed p values for the mean was based on a Student's t-test and the median was based on a Wilcoxon rank sum test of the degree distributions of genes within each category. This analysis indicates that host proteins required by influenza virus have significantly more interactions amongst each other than would occur by chance, and thus are likely to act as rate-limiting "hubs" in the flow of biological signals (d) A similar comparison was done to identify proteins that participate in known higher-order biomolecular complexes, as defined in CORUM, both for the entire human protein interactome and for influenza A virus host factors. P value is indicated for the enrichment of influenza host factors in the known biochemical complex dataset. These results indicate that influenza virus-host factors identified in this study are more likely to participate in higher order biochemical complexes, and that the virus recruits these complexes to facilitate its replication.
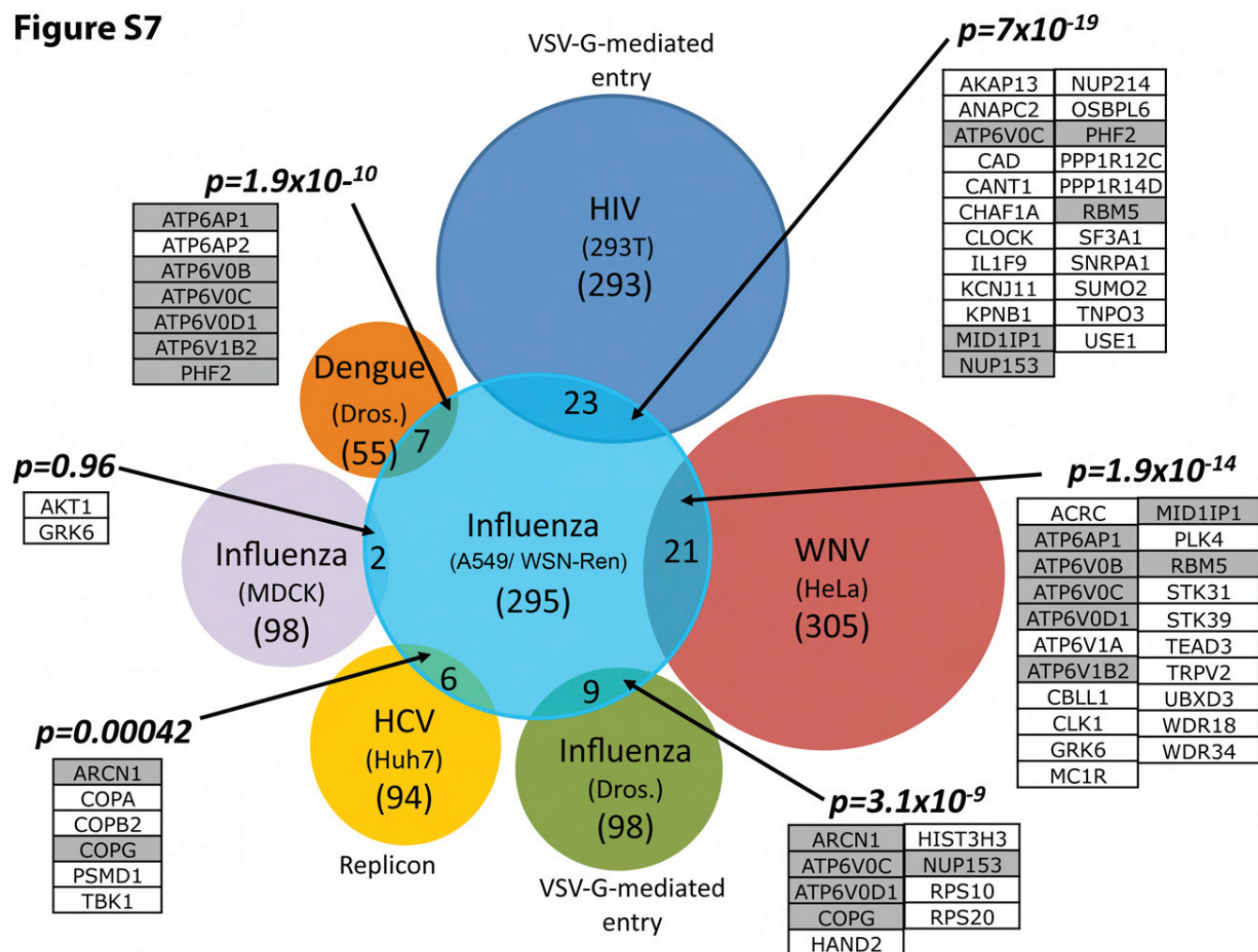
Figure S7

Figure S7. Overlap analysis of confirmed genes for influenza virus identified in this study with genes identified in other viral genome-wide RNAi/genetic screens. The 295 genes confirmed to be required for influenza virus replication in A549 cells are shown in the center. Factors confirmed by screens performed with HIV[4], WNV[5], influenza virus[8,9], HCV[6] and Dengue virus[7] are illustrated by the surrounding circles, which indicate the host cell system used and the number of genes identified in each case. Screens not performed with wild-type virus are noted. We performed a remapping of human orthologues to replace genes identified in the *Drosophila* screens. The number of genes common to both the A549/influenza screen and each of the other screens are indicated in the overlapping circles. The overlapping genes are identified along with the significance of the overlap (p values as determined by Chi squared tests), and those genes common to three or more screens are shaded. Note that this figure does not illustrate the overlap between the other screens; only those common to the influenza/A549 screen.
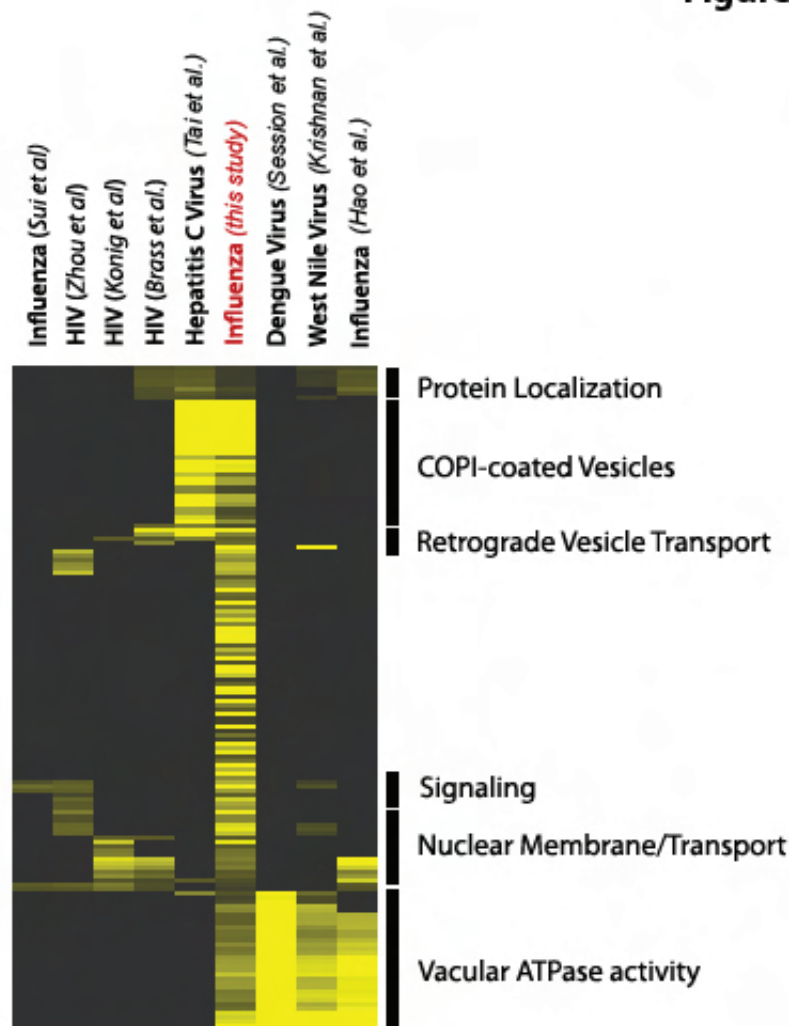
Figure S8. Figure S8. **Overlap and specificity of functional classes between viral host factors.** We analyzed the enrichment of Gene Ontology (GO) or Interpro (IPR) domain classes of host cellular factors reported to be utilized by the indicated viruses, and identified overlapping functional categories of host factors shared by the indicated viruses[4-9, 26, 27]. The colour intensity represents enrichment of a process by the indicated virus, i.e., yellow indicates a high degree of utilization of the pathway or process by a given virus, while black/grey indicates little or no dependence on the indicated pathway or process.
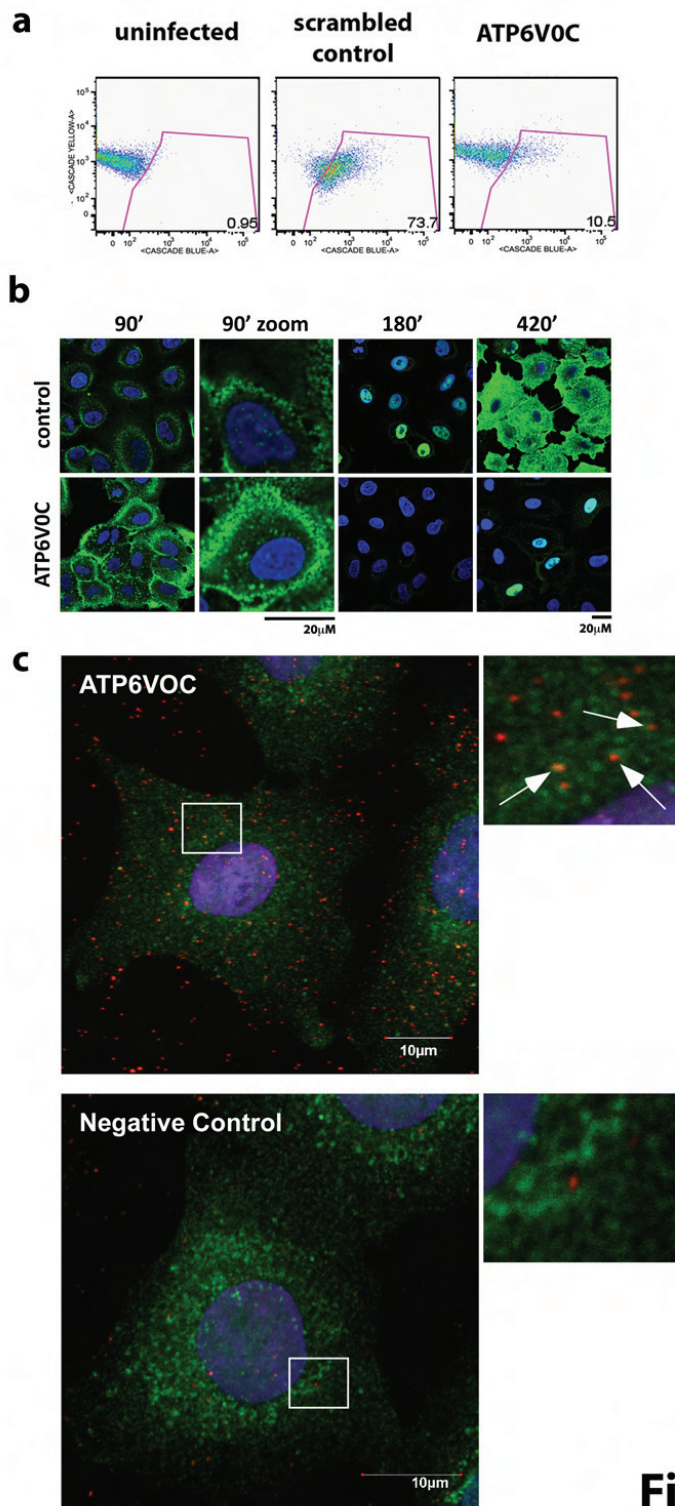
Figure S9

Figure S9. The vATPase subunit, ATP6V0C, is an important host gene for influenza virus entry. (a) To confirm the effects of vATPases on virus entry, influenza virus VLPs carrying a Bla-M1 fusion protein were used to infect A549 cells pre-transfected with the cognate siRNAs. The percentage of cells containing detectable cytoplasmic beta-lactamase activity is indicated. In cells transfected with a scrambled control siRNA, approximately 74% were infected by the VLPs as measured by

cytoplasmic beta-lactamase activity (second panel). However, depletion of ATP6V0C resulted in reduced VLP entry (10.5%), providing further evidence for the role of these proteins in low pH-dependent influenza virus entry. (**b**) Viral replication kinetics in control and ATP6V0C-depleted cells was monitored by tracking the localization of influenza virus NP protein. Cells were stained for NP (green) and nuclei (blue) and analyzed by confocal microscopy. At 90 minutes post infection an inhibition of incoming RNP accumulation in the nucleus was observed and a substantial delay in the appearance of newly synthesized NP both in the nucleus (180min) and cytoplasm (420min) was seen (**c**) Further confocal immunofluorescence analysis of HA (red) and Early Endosome Antigen 1 (EEA1; green) proteins in ATP6V0C siRNA-transfected cells (top panel) or negative control siRNA-transfected cells (bottom panel), 20 minutes after infection with WSN virus. The compressed z-stack images shown at 100X magnification are representative of at least 20 cells. Scale bar represents 10um. The increased number of HA-containing particles observed in the vATPase-deficient cells relative to the controls (n=199 versus n=90 in these examples) is likely due to a block to virus-cell membrane fusion. Approximately 19% (38/199) of the virions in the ATP6V0C siRNA-treated cells were judged conservatively to be co-localized with EEA1 (white arrows, insets), suggesting that they may be blocked within an early endosomal compartment.
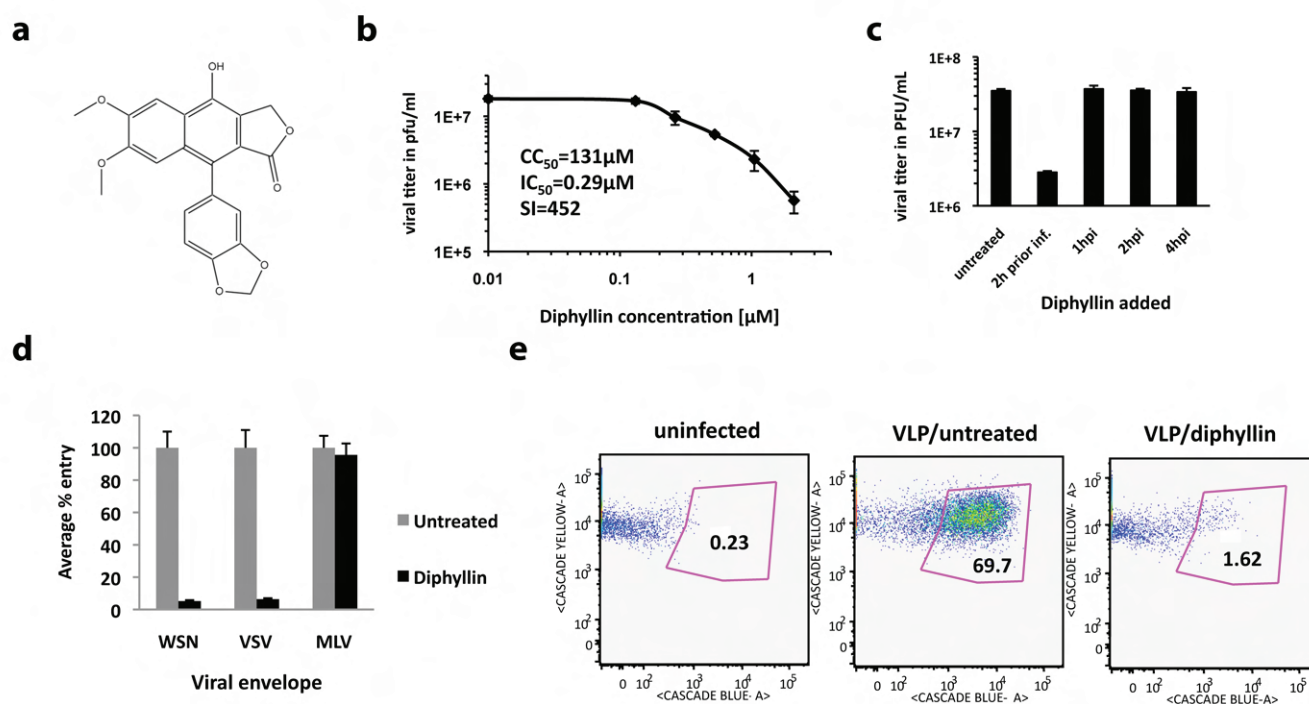
Figure S10. Diphyllin, a small molecule targeting vATPases [28], inhibits influenza virus entry . (a) Chemical structure of diphyllin. (b) Dose-dependent inhibition of influenza A/WSN/33 virus (MOI=1) by diphyllin in A549 cells. The concentrations for 50% cytotoxicity (CC_{50}), 50% inhibition (IC_{50}) and the selective index (SI) are indicated. (c) Kinetic analysis of diphyllin-mediated inhibition of influenza virus in A549 cells. Compound was added to the cells at the indicated times pre- and post-infection (MOI=1). Viral titers were determined at 24h. (d) Entry of the luciferase-expressing lentivirus particles pseudotyped with influenza virus (WSN), VSV or MMLV envelope in the absence or presence of diphyllin. (e) Entry of influenza virus VLPs carrying Bla-M1 in the presence of diphyllin. The percent entry is indicated.
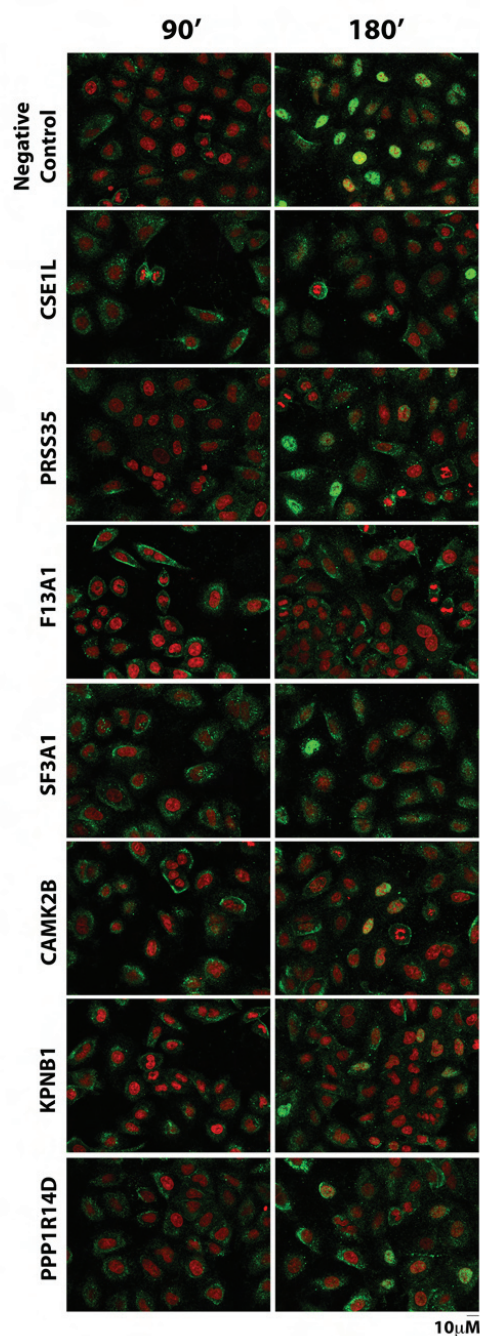
Figure S11. High content imaging of viral infection in host-factor depleted cells. The high-content imaging-based analysis was performed using the Opera (Perkin-Elmer, Waltham, MA), a fully automated microscope system. 384-well plates containing A549 cells were transfected with siRNAs targeting the indicating genes. 48h post infection cells were infected with A/WSN/33 virus and fixed at the indicated time points. After immunofluorescence labeling (see methods), cells were imaged using a 40x 0.9NA water immersion lens (Olympus), and representative images were selected. A total of 10-11 images for both the nuclear stain (Hoechst; red) and the Alexa488 labeled WSN-NP (green) were taken in each well.
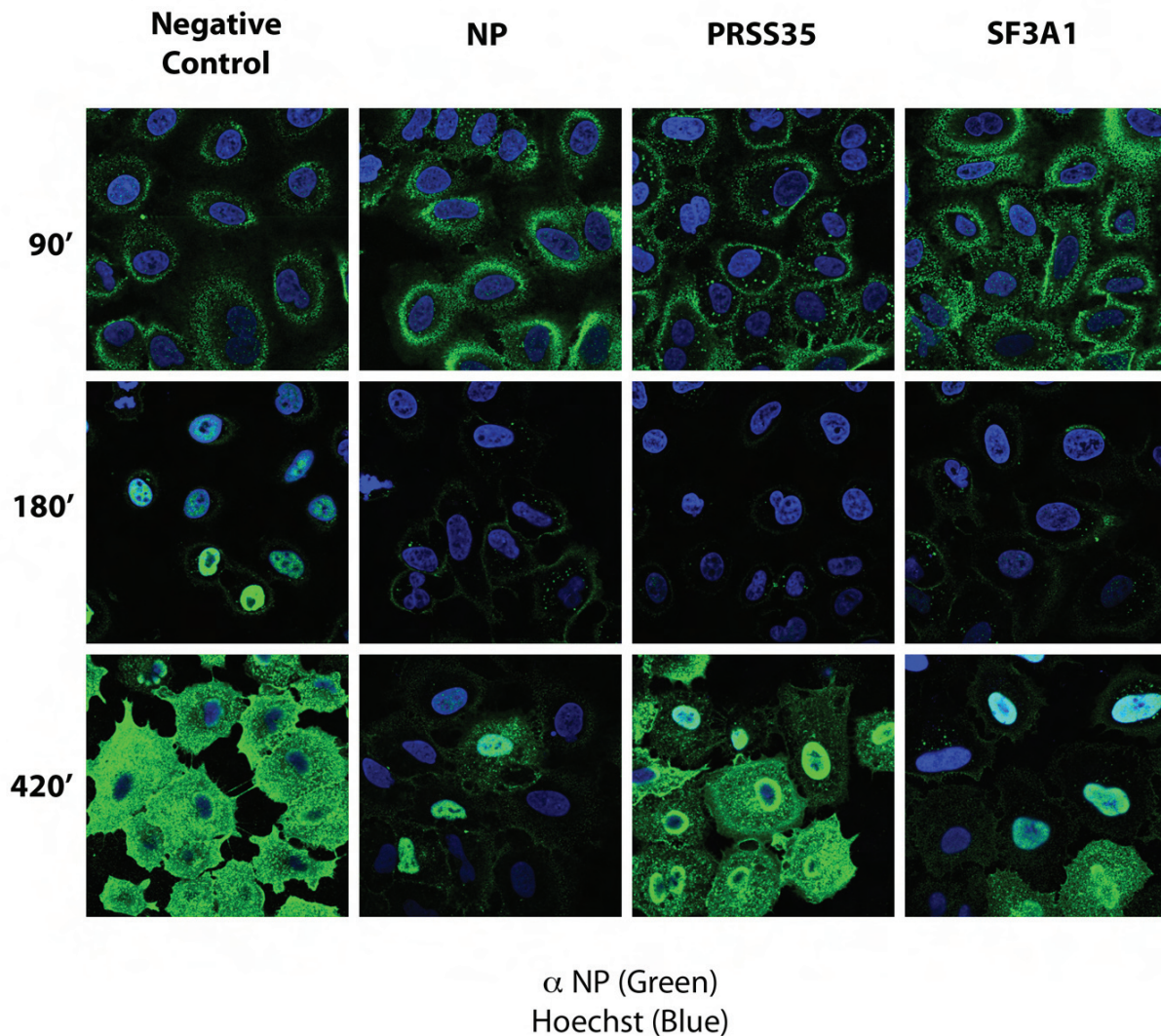
α NP (Green)
Hoechst (Blue)

Figure S12. Confocal imaging of influenza virus infected cells after host factor depletion. Additional confocal imaging at higher resolution was conducted to better visualize nuclear import of incoming vRNPs at 90' post infection. A549 cells pre-transfected for 48h with the indicated siRNAs were infected with influenza A/WSN/33 virus (MOI=10) and stained for NP (green) and nuclei (blue) at 90min, 3h and 7h post infection.
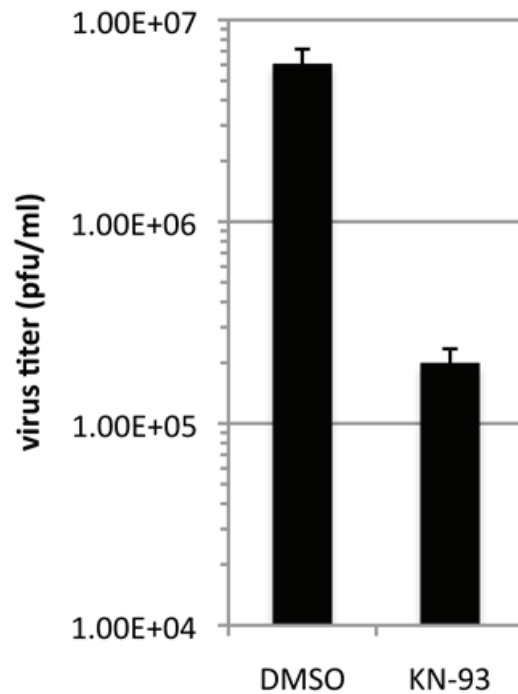
Figure S13. CAMK2B inhibition in A549 cells impairs influenza virus growth. A549 cells were infected with influenza A/WSN/33 virus in the presence of DMSO or 20µM KN-93. Viral growth was determined by plaque assay at 24h post infection. The mean viral titer +/- standard deviation of triplicate samples is shown. These data are consistent with the inhibition of influenza virus replication by KN-93 in MDCK cells (Figure 3d3e).

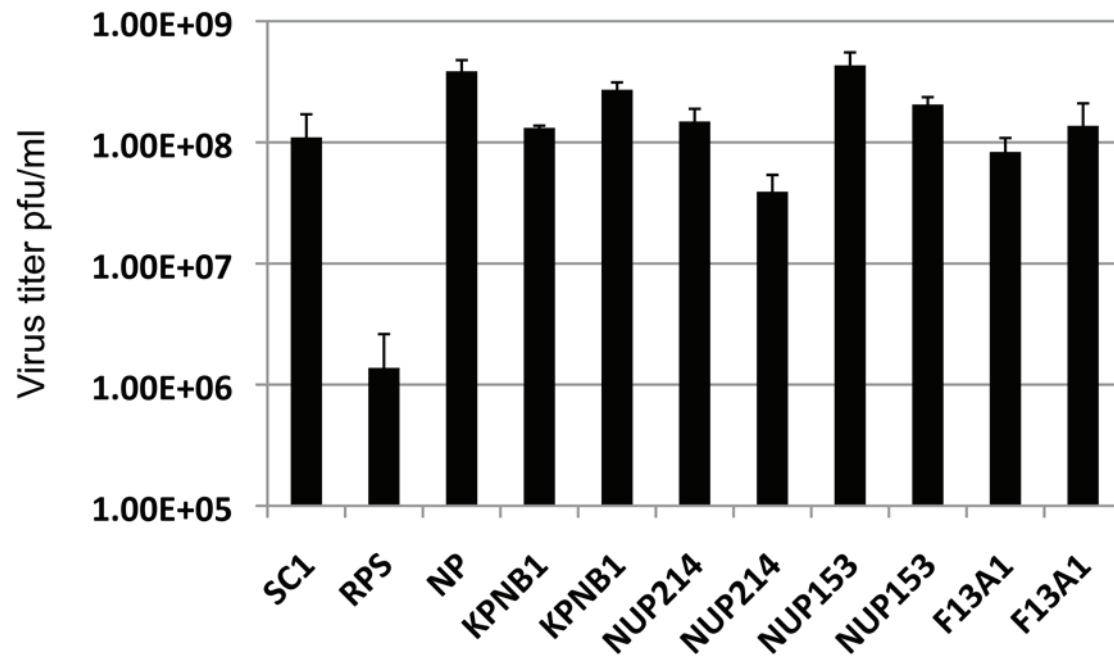**Figure S14. Additional effects of influenza virus host factors on VSV replication.** siRNA-transfected A549 cells were infected with VSV at a multiplicity of infection (MOI) of 0.01 at 48h post siRNA transfection. At 36h post infection supernatants were harvested and virus titers were determined by plaque assay on Vero cells. The mean viral titer +/- standard deviation of triplicate samples is shown.

Supplemental Table S1. Scores of 295 confirmed genes required for influenza virus replication. Explanation of column headings in table: *Gene_ID:* Entrez GeneID; *Symbol and Description:* Entrez Gene official Symbol and official full name; *GenebankID*: Refseq mRNA; *target sequence*: The best two siRNAs targeting each confirmed gene are shown; *Average*: mean of scores in reconfirmation assays at three different time points after infection: Renilla luciferase activity at 12h, 24h and 36h and Toxicity at 24h. *KnownViralPartners* and *KnownViralPartners_Indirect:* Influenza interacting protein as indicated based on literature search; *siRNA_SCORE:* evidence score calculated based on siRNA activity; *RSA_SCORE_LogP:* evidence score calculated based on Redundant siRNA Analysis (RSA) (see Methods section); SCORE_Network_Direct, SCORE_Network_Indirect*, SCORE_MCODE:* binary evidence scores if respective genes are contained in Network based on direct or indirect interactions or MCODE (Molecular Complex Detection analysis) respectively (1 or 0); *SCORE_OPI_Support*: evidence score calculated based on grouping in one of the OPI (Ontology-based Pattern Identification) functional categories (see Methods section); *SCORE_GOEnrich*: evidence score calculated based on gene ontology enrichment analysis; *SCORE_KnownViralPartners_Direct, SCORE_KnownViralPartners_Indirect :* Evidence score calculated based on direct and indirect interactions with influenza virus proteins respectively; *SCORE_DrugInformation:* binary evidence score on known drugs specific for respective gene; Calculations for each evidence score are described in Materials and Methods.

Supplemental Table S2. Overrepresented functional processes and protein domains of proteins required for influenza virus replication. Gene Ontology (GO) (http://www.geneontology.org) [1] or Interpro (IPR) domain classifications (http://www.ebi.ac.uk/interpro/)[2] found to be overrepresented within the 295 confirmed host cellular factors required for influenza virus replication are presented. Specifically, (A) GO or IPR accessions and (B) descriptions of these categories, as well as (C) GeneIDs and (D) gene names that fall within these classifications are listed. p values for each category were also calculated (E).

Supplemental Table S3. Functional classification of biological processes required for influenza virus replication. 295 confirmed factors were classified using the DAVID Gene Functional Classification tool (http://david.abcc.ncifcrf.gov), and this is graphically represented in Figure S2. The 11 broad categories are shown in separate tabs and each worksheet lists the genes (1st row) and functional categories (column A) utilized

for classification.1 indicates inclusion in a functional category, while 0 indicates exclusion.

Supplemental Table S4. Overrepresented functional pathways required for influenza virus replication. 295 host factors required for influenza virus replication were classified using the Ingenuity pathway (first tab) and GeneGo (second tab) analysis software (http://www.genego.com; http://www.ingenuity.com). This table lists the overrepresented pathways (A), significance (p-value) for each pathway (B) and gene names that fall into the respective pathway for Ingenuity (C).

Supplemental Table S5. References for selected functional categories presented in Table 1. Selected genes from the 295 confirmed host cellular factors required for influenza A virus replication depicted in Table 1 were assigned to the respective functional category based on analysis shown in supplemental tables S2, S3, S4 and various additional databases using the BioGPS tool (*http://biogps.gnf.org*); selected databases at BioGPS: NCBI-Pubmed (*http://www.ncbi.nlm.nih.gov/sites/entrez?db=pubmed*), NCBI-GeneRIF *(http://www.ncbi.nlm.nih.gov/projects/GeneRIF/)*, iHOP *(http://www.ihop-net.org/UniPub/iHOP/)*, DAVID bioinformatics database (*http://david.abcc.ncifcrf.gov/gene2gene.jsp)* , KEGG gene and pathway database *(http://www.genome.jp/kegg/)* and Wikipathways *(http://www.wikipathways.org/index.php/WikiPathways)* and geneWiki [3].**Functional Category**: selected functional categories; **References:** The table lists references for known roles for the cellular pathways in influenza virus replication.

Supplemental Table S6. Binary interactions of the host pathogen interaction map (Figure 1C, Supplemental Figure S4). 4,266 binary interactions between 181 confirmed influenza virus-host cellular factors, 10 viral nodes and an additional 184 cellular proteins that both showed activity in the primary RNAi screen (>40% inhibition) and harbour at least two interactions with at least 2 confirmed factors. Explanation of column headings in table: *GeneID, Symbol:* gene ID and symbols of binary interactors; viral proteins were assigned negative gene IDs, (-1 to -10); *SOURCE:* source of information, see Materials/Methods; *InteractionType*: type of interaction: direct interaction (pp) or indirect interaction (ppp). Viral nodes were abbreviated as follows: HA (Hemagglutinin), NS1 (NS1 protein), M1 (M1 Matrix protein), NEP (NEP/NS2 protein), NP (NP protein), PB1 and PB2 (the Polymerase subunits PB1 and PB2), PB1-F2 (PB1-F2 protein), vRNP (influenza viral ribonucleoprotein complex), virion (proteins incorporated into virions).

Supplemental Table S7. Overlap between viral host factors required by different RNA viruses. Host genes found in at least 2 viral RNA screens [4,5,6,7,8,9] are shown (column A-C). Host genes identified in this paper overlapping with those identified in other viral screens are highlighted in bold. Column D-J depicts the occurrence of the respective gene in either this study (column D) or other screens (column E-J). The number of times the respective gene occurs in different screens is shown in column K.

Supplemental Table S8. Biochemical complexes that are required by different RNA viruses. Underlying data/gene lists used to generate Figure 1d and Figure S8 are shown (first tab). Genes identified in this study (columns A-C) that belong to an overrepresented GO category (columns D,E) are listed. Columns F-O depict their utilization by several RNA viruses. Respective HIV and influenza virus datasets were combined for this analysis. Tab 2 indicates –Log(p) values used to generate Figure 1d, and Tab 3 includes percentage (number of reported host factors/number of proteins in complex) of the complex utilized by be each virus.

Supplemental Table S9. Host proteins confirmed to be required for wild-type influenza virus growth and gene expression. siRNAs targeting 294 host cellular factors (column A-D) were tested for their ability to inhibit wild-type influenza virus growth in A549 cells (MOI=0.01) as measured by hemagglutination assay at 36h post-infection. Reduction in HA titer (expressed as $\log_2$) for duplicate samples is shown in columns E, F and the average in column G. The number of siRNAs that meet the criteria for each gene are listed in column H. A call for a confirmed gene (see materials/methods) is indicated in column I. The ability of the siRNAs to inhibit viral gene expression was examined using qRT-PCR on NP (column J) and M1 (column K) mRNA at 6h post-infection. Controls were set to the value of 1. An average value of column J and K is shown in column L. A call for a confirmed gene (average value <0.65) is indicated in column M.

Supplemental Table S10. Examination of interferon induction in siRNA-transfected cells. A549 cells transfected with the indicated siRNAs were either mock infected (column G) or infected with influenza A/PR/8/34 virus (MOI=0.5) (column H). At 6h post-infection RNA was collected and interferon (IFN)-β mRNA was quantified by qRT-PCR. Control samples were set to 1. For reference, siRNA-mediated reduction in viral gene expression (average of NP, M1 mRNA) is shown in column F. A select number of siRNAs were also tested in an IFN bioassay to detect biologically-relevant amounts of IFN released from siRNA-transfected cells either mock infected (column I)

or infected with influenza A/PR/8/34 virus (MOI=3) (column J). Controls (shaded in blue) included: an siRNA targeting the viral NS1 protein as well as infection with a recombinant PR8 virus lacking NS1 expression. In both cases, this results in IFN induction. Furthermore a standard curve of recombinant IFN treatment is shown (shaded in yellow). ND=no data.

Supplemental Table S11. Evaluation of host factors that regulate influenza virus entry. A subset of siRNAs targeting factors shown to be required for efficient growth of wild type influenza virus (see Table S9), were evaluated for their effects on infection with pseudotyped lentivirus particles. Particles bearing envelopes derived from either influenza virus HA (WSN) (column E), Vesicular stomatitis virus (VSV)-G protein (column F) or Murine leukemia virus (MMLV) Envelope (Env) (column G) were examined. Additionally, the effects of host factor depletion on entry of an influenza virus-like particle (VLP) was also assessed using a b-lactamase (Bla)-M1 assay (see Methods section) (column H). Identified entry factors are marked with a Y in column I; post-entry factors are designated in column J.

Supplemental Table S12. Effects of host factor depletion on expression of an influenza virus mini-genome reporter. 293T cells were transfected with siRNAs targeting the indicated genes and transfected again 48h later with an influenza virus mini-genome reporter construct encoding firefly luciferase and expression plasmids for NP, PB1, PB2, PA. In addition a Renilla luciferase expression construct under the control of an SV40 promoter was co-transfected. The percent firefly (column E) and Renilla luciferase (column F) expression relative to the control (SC1) is shown.

Supplemental Table S13. Expression levels of host factor after siRNA silencing. siRNA transfected A549 cells were analyzed 54h post transfection by quantitative RT-PCR for the expression levels of 12 host genes found to inhibit WSN and SOIV (**swine origin influenza A/Netherlands/602/2009 virus)** replication (Figure 3e; columns A-C). The siRNA sequence is shown in column D. The efficacy of the siRNAs to target their cognate mRNAs for degradation was examined using qRT-PCR (column E). Negative controls were set to the value of 1. Standard deviation of quadruplicate experiments is depicted in column F.